EVALUATION OF ADDITIVE MANUFACTURING SIDE CHANNELS FOR NUCLEAR NONPROLIFERATION APPLICATIONS

A Dissertation
Presented to
The Academic Faculty

by

Kevin Le

In Partial Fulfillment
of the Requirements for the Degree
Masters of Science in the
Nuclear and Radiological Engineering

Georgia Institute of Technology
May 2021

COPYRIGHT © 2021 BY KEVIN LE

EVALUATION OF ADDITIVE MANUFACTURING SIDE CHANNELS FOR NUCLEAR NONPROLIFERATION APPLICATIONS

Approved by:

Dr. Steven Biegalski, Advisor
School of Mechanical Engineering
Georgia Institute of Technology

Dr. Christopher Saldana
School of Mechanical Engineering
Georgia Institute of Technology

Dr. Colt Montgomery
Research and Development Engineer
Los Alamos National Laboratory

Date Approved: April 30, 2021

Dedicated to my Grandparents, Dad, Mom and Sister.

ACKNOWLEDGEMENTS

I firstly would like to thank Dr. Steven Biegalski, Dr. Christopher Saldana, Dr. Colt Montgomery, and Mr. Michael Brand for their support throughout my academic journey. I also would like to pay thanks to my family who have given their unconditional support and have made significant sacrifices for me to be where I am today. Lastly, thank you to my friends from graduate school who have made the journey fun and exciting.

TABLE OF CONTENTS

LIST OF TABLES

LIST OF FIGURES

LIST OF SYMBOLS AND ABBREVIATIONS

3D	Three Dimensional
3DP	3D Print Process
AM	Additive Manufacturing
CSV	Comma Separated Value File
DMM	Digital Multimeter
EBT	Extrusion Based Technique
EFAB	Electrochemical Fabrication
FDM	Fused Deposition Modeling
FIBDW	Focused Ion Beam Direct Writing
KNN	K-nearest neighbor
LCVD	Laser Chemical Vapor Deposition
LOM	Laminated Object Manufacturing
ML	Machine Learning
NI	National Instruments
PCI	Peripheral Component Interface
PLA	Polylactic Acid
PXIe	PCI eXtensions for Instrumentation
SL	Stereolithography
SLM	Selective Laser Melting
SLS	Selective Laser Sintering
UI	User Interface

SUMMARY

The nuclear industry is continuing to grow and adopt new technologies to manufacture components. One of the technologies under consideration for adoption is AM. AM could make production of components cheaper and faster; however, it is prone to nuclear proliferation risks. Assessing the condition of component requires visual inspection; however, AM machines give off signatures that offer alternative means or side channels that give insight about the state of the component. There are correlations to be found between these side channels and these states. If correlations were found between the side channels and the geometry being manufactured, monitoring agencies could utilize these correlations for oversight. Proliferators could also take advantage of these correlations to steal nuclear technology blueprints. This work aims to explore the feasibility of using side channels to predict geometric characteristics of components being manufactured by AM machines. This work has been done on a Ultimaker 2+ 3D printer. The side channels that will be assessed are temperature, vibration, and current. The questions answered are: 1) how can time dependent temperature, vibration, and current correlate to specific geometries, 2) how can current predict the velocity of the nozzle, 3) how can vibration be used to predict the height of a geometry, and 4) how can vibration distributions be used to distinguish geometries from each other.

CHAPTER 1. INTRODUCTION

1.1 Motivations

In the nuclear industry, reactors are manufactured with specialized methods and training. These existing methods can contribute to higher costs thus there is the search to implement cheaper and faster alternatives. AM is a promising solution that eliminates the need for specialization as it produces complex components layer by layer instead of producing a complex component all at once. However, AM comes with major nuclear proliferation concerns. A major concern is how AM machines are not directly subject to export controls. AM machines can be circulated and end up in the hands of proliferators. If given the chance, proliferators could use AM to accelerate their own nuclear programs which could result in widespread nuclear material and nuclear weaponry. Another concern is how prone AM is to information leaks. AM has "side channels" in which proliferators can tap into and ascertain details about the geometric characteristics of the component being manufactured. These side channels pertain to signatures that AM machines give off with some examples being: temperature, vibration, power, and sound. Each geometry manufactured gives off their own unique signals, and proliferators can home in on that uniqueness to deduce exact geometric characteristics of critical nuclear components. If these side channels are left open, there could be rampant blueprint theft.

This work focuses on how AM side channels can be used to predict geometric characteristics. Understanding this process can help protect AM machines from being vulnerable to information leaks and can lead to remote monitoring efforts that can let authorities see if any critical nuclear componentry is being manufactured using AM.

1.2 Purpose

The goal in this thesis is to demonstrate that it is feasibility to use side channels to identify geometric characteristics of the component being manufactured via AM. AM represents a broad range of technologies; however, for this work the focus will be purely on thermoplastic extrusion-based methods.

The work will be done on a Ultimaker 2+ thermoplastic printer. The side channels that will examined are temperature, current, and vibration. A series of experiments were proposed and performed:

1) Time dependent temperature data will be analyzed for correlations to specific geometries
2) Time dependent current data will be analyzed for correlations to specific geometries
3) Time dependent vibration data will be analyzed for correlations to specific geometries
4) Current data distributions will be analyzed for correlations to specific geometries
5) Time dependent current data will be used to predict where filament has been placed on the substrate of the Ultimaker 2+
6) Time dependent vibration data will be used to predict the height of a manufactured geometry
7) Vibration data distributions will be analyzed for correlations to specific geometries

1.3 Format of the Thesis

Chapter 2 will present background and a literature review that will be needed to comprehend the work. Chapter 3 will pertain to work done with the temperature side channel. One experiment will be presented. Chapter 4 is based on experimental position data collection. Although not a side channel, it is worth including for the ideas the chapter presents. The chapter will present one experiment. Chapter 5 will pertain to the current and vibration side channels. Current and vibration are grouped together because in one experiment, current data and vibration data are collected in tandem. This chapter will present 6 experiments. Chapter 6 will be where concluding remarks will be made, and future work will be suggested.

CHAPTER 2. BACKGROUND

This chapter presents the background necessary for conducting research pertaining to AM side channels. Section 2.1 will give a definition of AM, the technologies and offers an overview of the technologies that fall under the umbrella of AM. Section 2.2 will explore research and applications of AM in the nuclear industry. The hope is to elucidate which AM technologies the nuclear nonproliferation community needs to focus on. Finally, the chapter will conclude with a brief overview of how side channels are currently being utilized.

2.1 Additive Manufacturing Technologies

AM does not refer to a singularly technology rather it refers to a concept: starting with a basic building unit and assembly those units into a desired geometry. There are many technologies fit the criteria. Vaezi et al. [1] presents a succinct overview of the current technologies and their strengths and weaknesses for applications in micro-AM. Please refer to table 2-1 for the strength and weaknesses of each AM technology and for the materials that are relevant to each. Even though this review is for micro-AM applications, this literature is still relevant for familiarization with technologies in the AM space.

Table 2-1 AM Technologies with Strength and Weaknesses [1]

Process	Strengths and weaknesses	Resolution (μm)	Materials
MSL	Complicated, yet well-understood and proven technology, high-resolution, suitable for volume production, suitable for true 3D microparts, high repeatability, and limited materials	2	Photocurable polymers; hydrogels; ceramics—PZT, alumina, and HA; and metals—WC, Co, Al, and Cu
MLS	Ability of multimaterial sintering, no support structure needed, suitable for true 3D microparts, facilities are required to provide fine powders and post-processing microparts have porosity, and high-temperature process	30	Metals—Ag, Cu, and Al; ceramics; molybdenum; and 316L stainless steel
3DP	Ability of multimaterial printing, suitable for volume production, suitable for real 3D microparts, low-temperature process, no support structure needed, low surface-quality microparts have porosity, and achievable minimum feature size limited to 200 μm	20	Metals and ceramics
Inkjet printing processes	Wide range of materials, ability of multimaterial printing, ability of writing in 3D space, ideal for deposition of biological inks noncontact easy material handling, sensitive process, fair repeatability, and support structure is needed for 3D microparts	20	Liquid with viscosity of 2–10 mPas (can contain small particles (CIJ)) and liquid with viscosity of 10–100 mPas (can contain small particles (DOD))
FDM	Easy process, ability of multimaterial deposition, low repeatability, high operating temperatures, commonly is used for microscaffold fabrication, and limited biological materials (in order to process high temperature)	200	Thermoplastics
LOM	Suitable for microceramic parts; fully dense microstructure (>99 %); high mechanical strength; internal, hollow-shaped cavities and channels; part shrinkage after post-processing; achievable minimum feature size limited to 80 μm; and post-processing facilities are required	50	Ceramics—alumina, silicon nitride, and zirconia and metals—316L stainless steel
FIBDW	High-resolution process, ability of nanofabrication, favorable for 3D fabrication, slow process, and sensitive process	80	Metals and insulators
LCVD	Multimaterial is possible; high-resolution process, low-deposition rate, and high-system complexity; high-temperature deposition; and controlled-atmosphere chamber is required	1	Metals and semiconductors
EFAB	Highly robust microparts, suitable for true 3D microparts and complex mechanisms without the need for assembly, favorable for medical devices, devices cannot be too large and have limited height (1.25 mm), and complete removal of sacrificial material is difficult in some cases	20	Valloy-120 (Ni–Co alloy), Edura-180 (electroplated Rh), and palladium

Each technology has a unique process associated with how it constructs geometries. Among the simplest is SL. SL is a technique that creates 3D geometries out of a photopolymerizable liquid. A beam of light is focused onto the resin where upon contact

the resin hardens. In the SL process, a laser hardens regions of resin to form a 3D shape in a layer-by-layer fashion.

Kruth et al. [2] gives an explanation about SLS and SLM technologies. They can be considered together as they are both laser-based techniques that act upon a bed of powder where the powder is the material the user wishes to manufacture their geometry with. SLS fuses powder together by selecting regions to for the laser to impinge. The SLM process is analogous to the SLS process; however, it deposits more enough energy to achieve a full melt resulting in a homogenous material. After sintering or melting the powder together into the desire shape, a new layer is constructed by laying down powder onto the existing geometry where then the sintering or melting process begins again.

3DP also describes a process based upon utilizing a powder bed. Instead of depositing energy, a binding agent is deposited onto the powder to glue powder particles together. After a layer has been bind together, a new layer of powder is spread where the binding process repeats.

The Inkjet Printing Process technique is most analogous to a how a printer works. Singh [3] offers a description of the process. Like in a printer, this AM technique utilizes an ink, which consists of the material, and solvent. It exists in a liquid state until it is ejected onto the substate of the AM machine. The solvent then evaporates leaving only the material of interest.

FDM and EBTs are probably the most well-known among consumers. It is characterized by deposition of melted material continuously onto a substrate. The nozzle is controlled to place material down in patterns in which eventually form a layer of the

overall shape. A new layer is created by depositing the melted material on top of the pre-existing shape.

As described by Zhang [4], LOM describes a process in which laser beams are used to cut strips of material into shape. These shapes are then superimposed to form the entire geometry. This technique is not considered a true AM technique because it depends upon cutting off excess material. Instead, it is considered because the process is done in layer-by-layer fashion.

FIBDW and LCVD both depend upon depositing energy into a gas containing the material of interest. Upon interaction, it causes a gaseous to dissociate from the material therefore laying down a thin layer on the substrate. These technologies can be considered together as they only differ in how they deposit energy. FIBDW deposits energy utilizing a focused ion beam while LCVD deposits energy utilizing a laser beam.

EFAB is a hybrid technique as it involves additive manufacturing and subtractive manufacturing. In this process there are two materials: 1) the structural material and 2) the sacrificial material. The sacrificial material is used to generate a mold. The mold is not pre-built but rather generated during the process. Material is deposited into the mold and where it will planarized once allowed to set. Upon completion, the mold will be removed via subtractive manufacturing leaving the desired geometry.

2.2 Additive Manufacturing in the Context of Nuclear

Now that a general understanding of AM concepts and AM technologies has been established, it is also important to examine the applicability of AM in the nuclear industry. Kroenig & Volpe [5] address both sides. They discuss the advent of 3-D manufacturing deeming it useful and attributing to low skill, low-cost contemporary manufacturing. Many organizations are participating in this trend, but of notice are the industrial organizations that produce products for the defense industry. With these capabilities comes the concern that the technology may be used to support a nuclear program (i.e., manufacturing a gas enrichment centrifuge.) Export controls are currently in place to prevent proliferation, but AM machines could bypass these export controls since they are not subject to direct export controls. It is not only easy to obtain the necessary equipment but potentially one could gain access to sensitive files (i.e. design for centrifuge) through means of a cyberattack. These attacks would almost be unnoticeable. There has been work done to curb the spread of technology, but countries should still come together to impose restrictions and controls. There should also be efforts put into improving cybersecurity systems to prevent information from being leaked. Lastly, sales trends of AM machines should be tracked.

2.2.1 Proliferation Capability of AM

It is important to learn about the applicability of AM in the nuclear industry, so that an idea about proliferator capabilities can be developed.

Bergeron et al. [6] investigated the concept of 3D printing a nuclear fuel, specifically thorium dioxide. Commercially available SL printers were used alongside sintering methods to manufacture thorium oxide cubes with a ~95% theoretical fuel density. The

process included a resin burn out step (0-500 C) and the sintering process was done in air for approximately 2 hours at 1700 C. Parameters that were monitored throughout the process included density, surface roughness, impurity levels and microstructures. This study was able to produce thorium oxide at ~90% theoretical density with rougher surface finishes. A shrinkage of 18-23% was observed after the sintering process and cracks (possibly caused during heating) were observed. Impurities levels (i.e., resin and other impurities: carbon and tin) were compared and found that postproduction impurities concentrations had dropped relative to pre-production.

Bertsch et al. [7] investigated how ceramic components could be made using stereolithography. They utilized two methods. One method used alpha-alumina particles in a colloidal mixture. The mixture essentially was resin that could be used with typical SL printers. After printing, the components would undergo a process when the suspension medium of the alumina would be removed, and the alumina would be sintered together. The second method utilized a paste instead of a resin. The paste has been modified to have a high percentage of ceramic powder. Since the are using a paste, they required a unique printer that can spread the paste across the substrate. This paste is still photosensitive. Both techniques were able to produce the desired component; however, both components underwent significant shrinkage.

Gonzalez et al. [8] investigated 3DP technology for use in creation of ceramics. They used an aluminium oxide grinding powder in combination with an ExOne M-Lab system to manufacture components. Within the printing process, the depth layers (size of particles) were varied by purchasing grinding powders of different grits. In addition, a series of tests where the powders were uniformly mixed were performed. After printing, the components

were subjected to two different sintering schemes (2h and 16h). Characterization of density, shrinkage, morphology, microstructures, compression strength, hardness, and dielectric constants were performed through means of physical measurement, scanning electron microscope, X-ray diffractometer, and hydraulic systems. The mixed powder experiments produced components that achieved 96% of their theoretical density. It was concluded that "the increase in powder distribution and smaller layer thickness provided the best results." All parts that underwent sintering underwent noticeable shrinkage. It was also hypothesized that these high density components could be used as protection in harsh environments.

Bandyopadhyay et al. [9] investigated manufacturing with ceramic materials using FDM. Two methods were employed: 1) direct FDM manufacturing of the component, and 2) indirect manufacturing which involved FDM manufacturing the mold of the component. The study dealt with lead zirconate titanate (PZT), a piezoelectric material. In direct manufacturing method, filaments containing PZT were not commercially available, so a method was developed to embed PZT (50-55 vol% PZT) within a commercially available thermoplastic binder. The second method required printing a thermoplastic polymer negative image of the component. A ceramic slurry containing (high loading of PZT) was then deposited into the mold. A three-stage burnout of the binder was developed to suit the needs of the direct and indirect FD manufacturing techniques. To test the built components, electro-mechanical properties, series and resonant frequencies were all characterized.

Jialin [10] investigates production of nuclear materials with the use of SLS AM. The material chosen was V-6Cr-6Ti since it is an attractive nuclear material due to its temperature resistance, irradiation resistance and compatibility with liquid metal. An alloy

powder concentration of "88% V, 6% Cr and 6% Ti" was used. In preparation, the powder was milled into as close to perfectly spherical balls where mill times were selected to be 5, 10, 15, 20, and 25h. SLS was performed by the "EOSINT M 280." It was decided to use a laser power of 195W, a scan speed of 700mm/s, and a "powder" layer thickness of 40 microns. Characterization tools included a scanning electron microscope, an x-ray spectroscope, and CMT5205 compression testing machine. The results of milling after 25h appeared to almost spherical particles of the alloy and was relatively uniform. The SLM components had a smooth finish and around 98% of the theoretical density. Two common microstructures (columnar dendrites and cellular grains) were observed. The microstructure spacing between the columnar dendrites and the cellular grains appeared to be less than 1 micron.

2.3 Utilizing Side Channels in Additive Manufacturing

With a brief overview of applications of AM in the nuclear industry, it would make sense to look at how side channels are being used to "tap" into these AM technologies. It will become apparent that side channels are not purely physical (i.e., temperature, power) rather they refer to any means that allow access to information about the AM machine.

Al Faruque et al. [11] has developed an attack method utilizing the temperature side channel. They accessed the temperature side channel by placing a thermal camera facing the XZ or YZ plane of the 3D printer. The thermal camera was responsible for tracking the changes in the X, Y, and Z direction caused by the printer. The goal was to feed this data into mapping algorithms that can predict the activity of the printer. That activity can then be used to predict the exact g-code sequence the printer followed. The method failed to be

able to reproduce accurate results due to limitations imposed by their camera. These limitations include a low resolution, and a low image capture frequency. Even though they failed, they mentioned using the temperature side channel, especially thermal images, is still viable given that a higher quality camera is used.

M. A. Al Faruque [12] investigated the use of the acoustic side channel to reconstruct g-code sequences for the geometries the AM machine is producing. They collected the acoustic data using a cellular device, and then extracted it from the phone for post-processing. Post-processing included feature extraction so that they made be fed into regression and classification models. They also utilized another model that predicted direction of the nozzle. Utilizing all outputs provided by the nozzles, they would construct the g-code sequence. They focused on reconstructing a square, a triangle, and a complex shape.

Wu et al. [13] investigated machine learning methods using static camera images for detecting cyber-physical attack occurrence within additive manufacturing. They used multiple machine learning algorithms (KNN, random forest and anomaly detection) in combination with a extrusion nozzle mounted camera and a static camera. Several defect cases were used: seam defect, irregular polygon defect, circle defect, rectangle defect, and triangle defect. Simulated images and camera images were used with each image evenly split into eight sections pertaining to 32,768 pixels. Analysis involved utilizing grayscale features in each section ("mean of grayscale in each section, standard deviation of grayscale, and number of pixels grayscale larger than 120"). Anomaly detection methods were able to identify an attack 96.1% based on static camera images.

Sturm et al. [14] stated the importance of future additive manufacturing systems and how they are becoming increasingly integrated into network systems. Examined in the paper were possible cyber-attack vectors, such as a CAD model, a STL file, a toolpath file, and the machine hardware, that could be used to affect physical attack components. A case study was performed using an STL file in which a void insertion attack was used. "ASTM Standard D638-10 tensile test specimen was printed via Powder bed Fusion" with and without voids. Finite element analysis collected data on Von Mises Stress and revealed that dogbones with voids were unnoticeably different from dogbones without voids, but the voids still caused the dogbones to fail.

Li et al. [15] utilized machine learning to predict the surface roughness of components produced by desktop printer MakerBot Replicator Plus. They extracted temperature of the build plate, temperature of the extruder, vibration of the build plate, vibration of the extruder, and temperature of the material deposited (tracked with IR sensor). They used an ensemble ML method. An ensemble ML method can be thought of combining multiple algorithms each trained in their own unique situations, and these algorithms can be of the same or different types. In this instance, random forest algorithm was used to extract features based on importance and then used in another ensemble algorithm for prediction. To incorporate each algorithm, they utilized a weight function in which a loss function was used to train. They trained using selected features and optimized weights. Those optimized weights are then used in the prediction algorithms. They used, random forest, adaboost, classification and regression tree, support vector regression, ridge regression and random vector functional link networks. All algorithms would output a prediction and weights would be applied to each prediction to make an overall prediction.

CHAPTER 3. TEMPERATURE STUDIES

3.1 Motivations

The first side channel of interest is temperature. The printer offers two means of for gathering temperature information. The nozzle and the substrate change temperature in response to the printing process. This first experiment acts under the assumption that these two temperatures time profiles are unique to the geometry that generated them. A novel collection method and studies have been designed to prove that temperature is a viable side channel for deriving the geometric characteristics of a manufactured object.

3.2 Methodology

3.2.1 Equipment

The AM machine of interest is the Ultimaker 2+. This printer offers an open design making embedding sensors simple, and basic USB connectivity for interfacing with the printer. The printer itself consists of a nozzle powered by an x motor and y motor, a glass substrate powered by a z-motor, and temperature controls for both the nozzle and substrate. On the back of the Ultimaker, the filament roll is held in place. The Ultimaker 2+ is displayed in figure 3-1.

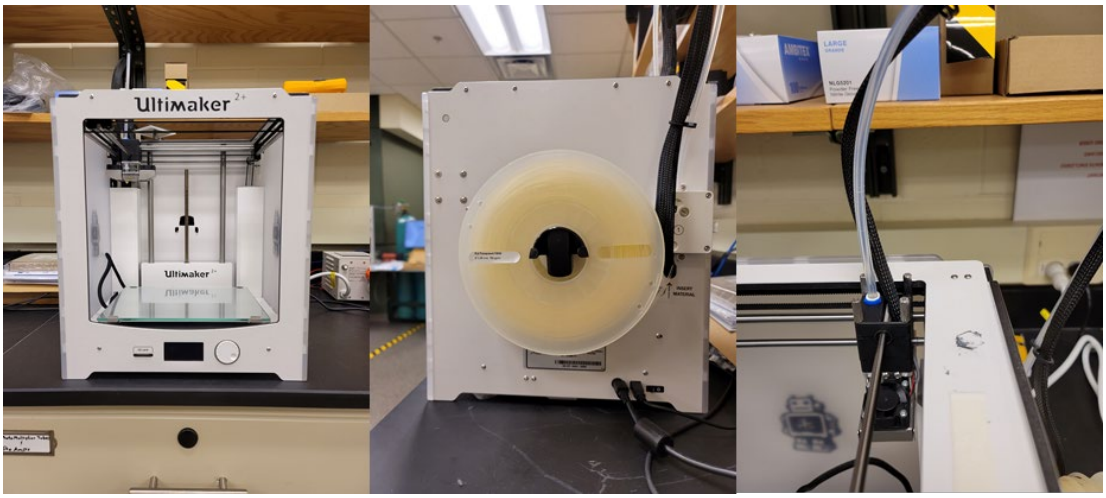

Figure 3-1 Ultimaker 2+ System

The filament is feed into the nozzle via the feed motor. The nozzle houses a heating element which melts the fed material. During printing, the nozzle moves in the x-direction and y-direction, while the substrate lowers and raises emulating z-direction movement.

The print settings for all experiments are as follows: they were made from transparent ultimaker 2+ branded PLA, the layer height was set to 0.1 millimeters, the infill density was set to 10%, and support was turned on, and adhesion was turned on. Layer height refers to the thickness of each layer. The printing process occurs in a layer-by-layer fashion, and it is possible to designate the how tall a layer is. Smaller layer heights, the more stability but it will take longer.

When 3D printing, it sections the component into two areas called the “shell” and the “infill.” The shell refers to the material used to outline the body of the component. Infill refers to how dense the inside of the component is. The infill setting is designated by a percentage, and the higher the density percentage the stronger the component will be. Support refers to printing additional structures to hold up the component. This is essential AM needs a base to print off since it cannot print in midair. Having adhesion turned on means the print process will start by producing a layer that rest of the geometry will sit on.

The layer is meant to act as a bind between the print and the substrate. The component can warp and bend in the printing process and adhesions can help mitigate it.

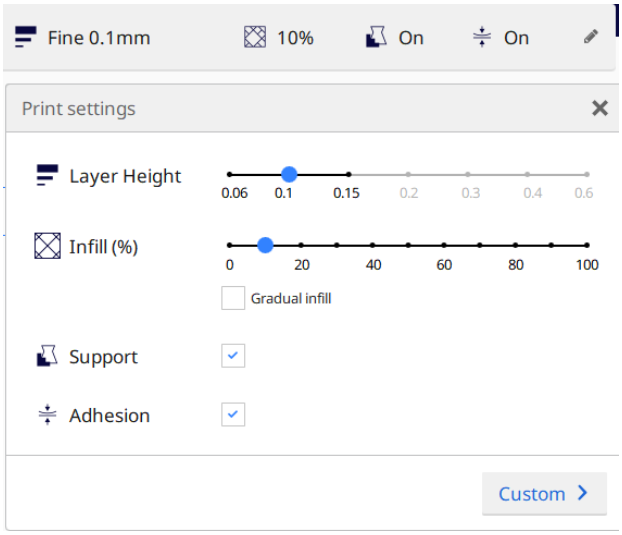

Figure 3-2 Print Configurations for Ultimaker Cura 4.3.0 Software

An external computer was setup adjacent to the printer and connected to the ultimaker 2+ via USB 3.0. The computer was loaded with third party print monitoring software Pronterface and custom Python scripts. More information about Pronterface and Python usage will be given in the data collection section.

3.2.2 Data Collection

There was a need to find a software that could track and export temperature information. A candidate was CURA, an Ultimaker proprietary software that can slice geometries, and can monitor the temperature of the nozzle and the temperature of the bed. Although it did have temperature monitoring, there was no direct way to extract nozzle the temperature information using CURA. After additional searching, Pronterface was eventually settled upon.

Using Pronterface, Python version 3.7, and Python libraries a novel data collection method capable of extracting temperature of the nozzle and temperature of the bed was able to be designed.

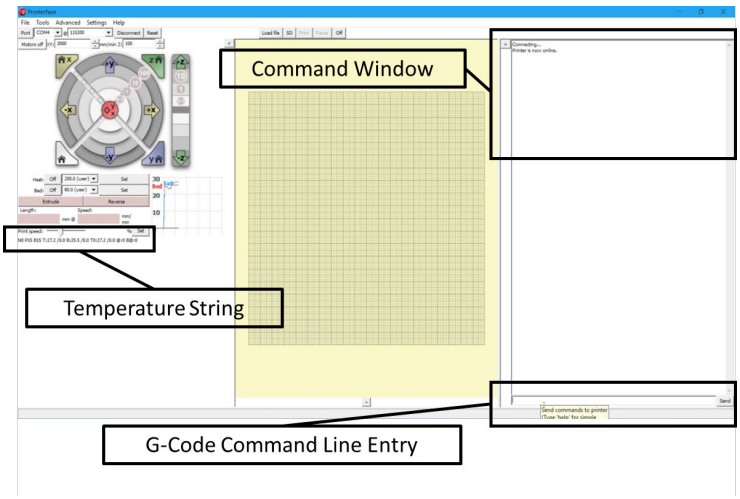

Figure 3-3 Pronterface Software UI and Highlighted Relevant Information

"Pronterface" is a Python-based generic 3D printer interface for FDM machines. It can monitor both the printer nozzle and the printer substrate. Pronterface was also attractive because it included controls to move the nozzle and move the substrate. There are two methods to control the printer. For this study, the most significant part of the UI was a textbox that displayed the temperature of the nozzle and the temperature of the substrate. The middle of the Pronterface window offers a place where geometries can be displayed and sliced. On the right side of the UI, there was a command window and a G-Code command line. These features were important for future studies. For this study, only the temperature strings, was considered.

Python 3.7 was used due to the researcher's familiarity with the language and its diverse libraries to draw from. With no way to extract the data explicitly, an option was to parse the data from the Pronterface window. A library called "Pywinauto" was used. It offers modules that help in automating interaction with applications in the Windows

operating system. The capabilities of interest were being able to parse text strings, take control of menus inside an application, insert strings, and click buttons. How Pywinauto was utilized in code will be provided in appendix section 1**.** Parsing capabilities are used to extract the temperature strings. The last three capabilities were important for future studies.

The temperature of the nozzle and the temperature of the substrate were displayed as strings inside Pronterface which made parsing the temperature data easy. After parsing, a variable inside the python script would hold the string where then the temperature string and a generated timestamp would be appended to a file. The timestamp was generated based on unix epoch time. This loop was repeated for a user designated amount of time.

3.2.3 Experimental Process

The geometries used in this study are a 1x1x1cm cube and r=.5cm, z=1cm cylinder. Each will be manufactured three times in sequence which will result in six total datasets. Three cubes were printed first followed by three cylinders.

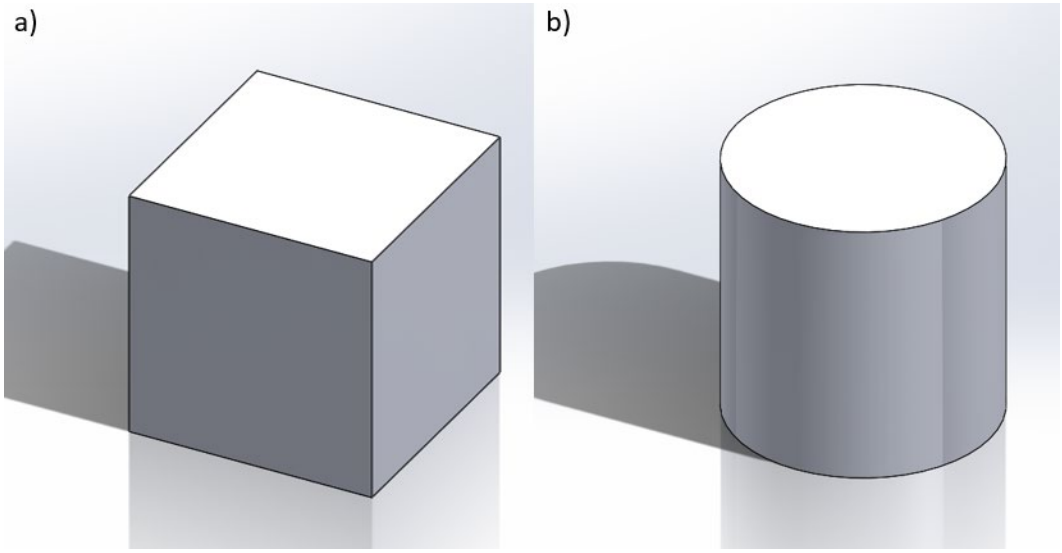

Figure 3-4 Geometries Used in Temperature Studies a) 1x1x1cm Cube modeled in Solidworks CAD Environment, b) r=.5cm z=1cm in Solidworks CAD Environment

A human operator will start the sampling of the process when the Ultimaker 2+ nozzle reaches 195 degrees Celsius. The collection process will continue until the system has completed returned to the idle state which in this case is where the nozzle has settled into coordinates x=0, y=0, and the substrate has settled into z=0. Stopping the collection process was also the human operator's job.

3.2.4 Data Processing

Before analysis, the datasets needed to be preprocessed. This is because the cube geometry took longer to print compared to the cylinder geometry resulting in datasets of unequal length. This meant the cube datasets had to be truncated to match the length of the cylinder dataset.

3.3 Results

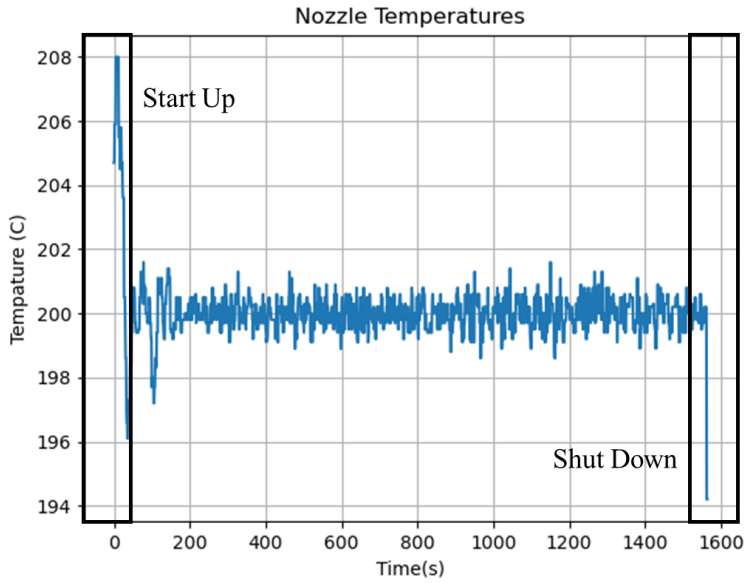

Figure 3-5 – Temperature Series Displaying Startup and Shutdown Signals

Initial visual analysis revealed that there were already a few patterns emerging from the data. It was possible to distinguish the startup and shutdown sequences for the printer from the rest of the dataset. This phenomenon is highlighted in figure 3-5.

Next the datasets were superimposed to glean if similarities existed between like geometries. Two cube data sets were superimposed in figure 3-6. What was expected was that the two profiles would match at each timestamp. What was observed was that the datasets appeared similar at some points and dissimilar at other points. To qualify this analysis, a comparison scheme called absolute differencing was developed.

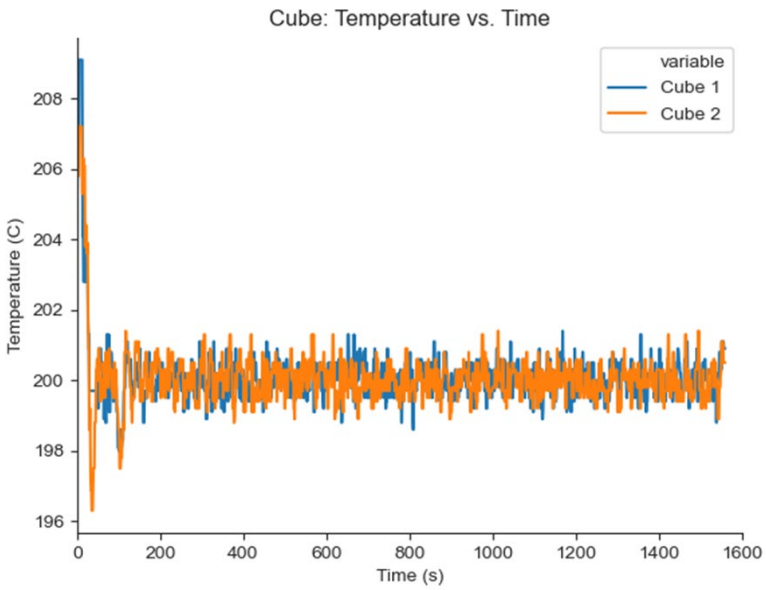

Figure 3-6 – Superimposed Time Series for Two Cube Datasets

3.3.1 Absolute Differencing

To reaffirm the notion that there was no uniqueness to be found within the temperature side channel in the Ultimaker 2+ nozzle, an absolute differencing analysis was

conducted. The method was thought of as a simple way to qualify the differences between two temperature datasets. This study acts under the assumption that for each timestep, there is a unique temperature value. Therefore, this method utilizes point by point comparison. The differences between two datapoints would be subjected to absolute value and then added to a total sum of errors. An algorithm was developed in Python 3.7 that would perform the process described above.

Table 3-1 Absolute Differences Between Geometries

	Cube 1	Cube 2	Cube 3	Cylinder 1	Cylinder 2	Cylinder 3
Cube 1	X	885.5	881.9	831.4	923.1	922.5
Cube 2	885.5	X	866.6	856.1	1063.2	971.8
Cube 3	881.9	866.6	X	799.3	942.4	945.4
Cylinder 1	831.4	856.1	799.3	X	895.9	820.3
Cylinder 2	923.1	1063.2	942.4	895.9	X	972.4
Cylinder 3	922.5	971.8	945.4	820.3	972.4	X

There were 14 combinations tested which involved like and dislike geometries being compared to each other. What was expected was to observe the like shapes would have lower differences when compared to each versus when dislike shapes were compared. The lower the difference, the more alike they were considered in this comparison method. Overall, when comparing cubes to cylinders, the differences seem to be higher. This may

indicate that there are patterns to find within the temperature side channel data within the Ultimaker nozzle. However, there were some notable exceptions. The most blaring case was cube 3 versus cube cylinder 1 with a difference value of 799.3. This is the lowest difference observed indicating that this analysis method considered these two shapes are the most similar among the datasets. Another notable comparison was between cylinder 2 and cylinder 3 which had a difference value of 972.4 which is among the highest observed differences. This analysis method determined that these two geometries were among the most dissimilar even though they were both cylinders. These cases contradict the expected results which may suggest some complications.

3.3.2 Distribution Comparison

To take the analysis one step further, the time series were collapsed into relative frequency distributions. Using relative frequency offers a mean of normalized comparison since some objects take longer to manufacture than others. The point of comparing distributions is that specific bins in the relative frequency distribution will correlate to the geometry that generated that object.

These distributions were superimposed and visually inspected. Cylinder and cube relative frequency distributions were superimposed and visually inspected. In figure 3-7, the cube dataset 1 relative frequency distribution (blue) was superimposed on top of cylinder dataset 1 relative frequency distribution (green). When examining the plots, all comparisons looked similar with differences being minute.

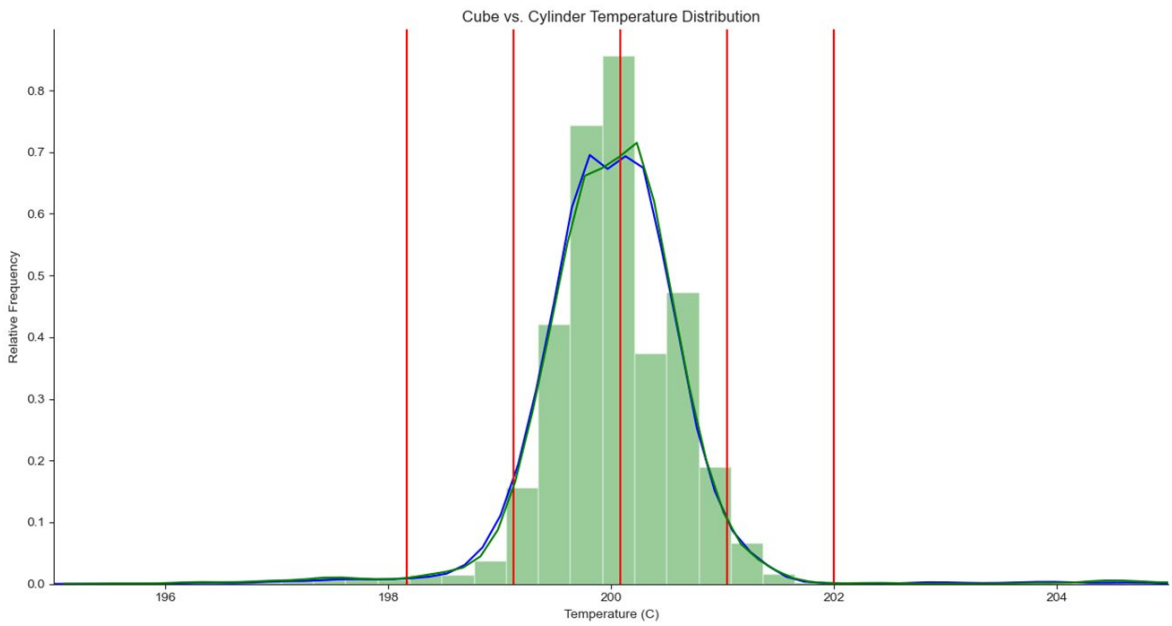

Figure 3-7 Cube and Cylinder Relative Frequency Distributions Superimposed

3.4 Conclusions

Instead of progressing further with distributions, it was decided that a better sampling system was needed to get usefulness out the temperature side channel from the Ultimaker 2+. Thus with this sampling method, the results pointed to the fact that the temperature side channel within the Ultimaker 2+ nozzle doesnot contain data that can be used to identify the geometry. There were some limitations and complications to learn from for future experiments.

The first is the limitation imposed by a low sampling rate. The data collection method described was able to collect temperature data at one sample per second because Pronterface only updated the temperature string once per second. In low sampling rate system, it may be possible to "miss" the essential parts of the data meaning that data that was unique to the geometry may have been missed. Thus, signals observed would have

little continuity. A higher sampling rate could expose the intermittent points and affirm if there are patterns to be discovered in the temperature time-series that are unique to the geometry that generated it.

Secondly, misalignment may have occured because of human initiated sampling. There was no way to ensure that t=0 for all datasets was properly aligned due to inconsistent sampling starts.

Finally, there were thoughts the observed temperature behavior may be influenced by a static temperature controller rather than having the temperature change being influenced by the geometry the machine is producing. The Ultimaker 2+has the ability to adjust it nozzle speed mid process to ensure proper deposition of material. Therefore, it would not need to change temperature to adjust the deposition rate. The nozzle in this scenario would only need to maintain a constant temperature.

CHAPTER 4. PRELIMINARY POSITION DATA EXTRACTION STUDIES

4.1 Motivations

Earlier it was mentioned that Pronterface is attractive for its command line. The Pronterface command line was used to extract the Ultimaker 2+ nozzle coordinate history due to an early idea that a model could be produced to predict if material had been placed in space. The model would accept side channel data such as temperature, current, and vibration, and predict if material has been placed at the coordinate the side channel pertains to. With the idea for the model in mind, it was essential to see if coordinate histories could be obtained through the Pronterface-Python sampling method.

4.2 Methodology

4.2.1 Data Collection

The Pronterface-Python sampling methodology was once again employed. Referencing figure 3-3, on the right side of the interface there is command window and an embedded g-code command line. Interacting with the command line allows the printer to receive instructions and gather information from the command window in real time. The most significant capability of the g-code command line is that it allowed for the position of the nozzle to be retrieved real time after inputting the “M114” g-code command. After the command was issued, the x and y coordinates of the nozzle, and the z coordinate of the bed were displayed in the command window. Those coordinates also existed in the form

of strings, so custom python scripts were modified to parse directly from the command window.

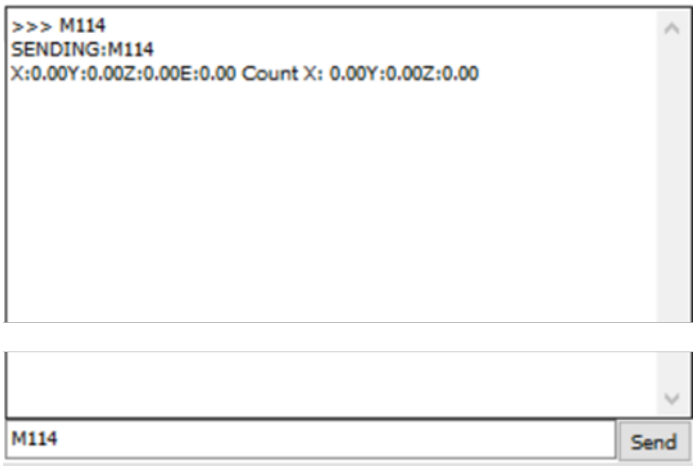

Figure 4-1 Example of Pronterface Command Line Being Used to Retrieve Position of Nozzle by Using M114 Command

The script utilized Pywinauto Python library. Aforementioned in Chapter 3, the capabilities of interest inside Pywinauto are being able to parse text strings, take control of menus inside an application, insert strings, and click buttons. The insert strings functionality was used to write "M114" into the command line which returned the current position coordinate of the nozzle. To send the command, the click button functionality was used to click the "send" button. A text string displaying the X, Y, and Z coordinates of the nozzle would be returned. The parse functionality would then extract the coordinate string from the command window, and then the string would be assigned to a variable inside the Python script. The position string would be appended to a file. This process was done repeatedly for a designated amount of time set by the user.

Continuous sampling was difficult due to the way Pywinauto operated. Pywinauto needs to identify the text box it needs to interact with each time it goes to input a string.

Pywinauto would have no clue which textbox to interact with unless the user specifically designated it. Therefore, the word “Here” was typed manually into the command line to help Pywinauto locate the correct textbox to interact with each time a request for coordinates needed to be sent. An example is provided in figure 4-2.

Figure 4-2 The Word “Here” in Pronterface Command Line

After locating the textbox, the script would save the textbox to a variable so Pywinauto would have always have access to it. Now the script could now interface and send the M114 command whenever coordinates of the nozzle were requested.

4.2.2 Experimental Details

The experiment produced two variations of the 1x1x1cm cube geometry (refer to figure 3-4a). The first variation was a 10% infill cube and the second variation was a 100% infill cube. Both geometries were printed once where nozzle coordinate histories was tracked and exported. The human initiated sampling started when the Ultimaker 2+ nozzle reached 195 degrees Celsius and stopped when the system has completed returned to the idle state. The idle is defined as the nozzle and substrate being in the coordinates x=0, y=0, and z=0. Two set of coordinate histories were produced.

4.2.3 Analysis

The analysis occurred by plotting coordinate histories using Python library matplotlib's scatter plot function. It produced interactable 3D graphs which made analysis possible.

4.3 Results

The position could be collected with limitations. This method was able to coarsely track the entire coordinate history from startup to the shutdown process. Essentially, it was able to loosely trace out the geometry.

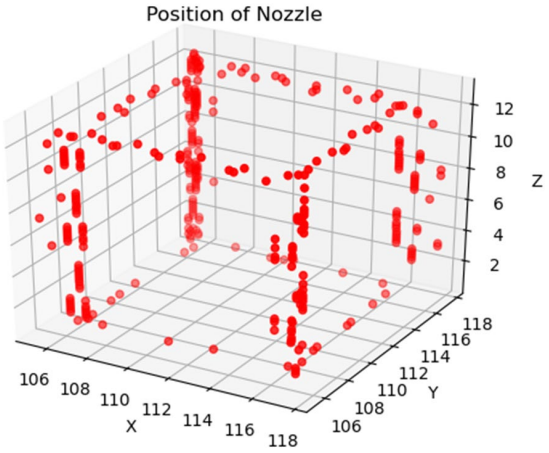

Figure 4-3 Coordinate History of the Nozzle During Printing of 10% Infill 1x1x1cm Cube

A glaring issue presented in fig 4-3, was that it was unable to collect any position data pertaining to the interior of the cube. It seemed to only be able to collect the position data seem pertaining to the edges of the geometry. Also, of note were that there was no

data collected about the side walls of the cube. The differs from the 100% infill object in figure 4-5 in which many wall points were collected.

Examining the geometry from the top revealed some “flaring” outside the bounds of the printed geometry. This can be clearly seen in figure 4-4. The flaring observed happens past the confines of the geometry end. A possible explanation may have to do with the fact that g-code files are processed serially meaning that only one instruction can be processed at a time. While the nozzle is past the confines, it is currently not receiving any direct instructions relating to the geometry, thus freeing the Ultimaker to process any nozzle position requests. This may suggest that these coordinates do not actually pertain to the shell of the geometry but rather these coordinates represent nozzle positions outside the confines of the cube.

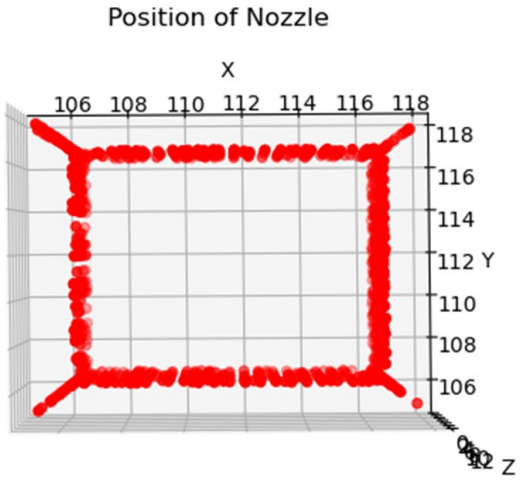

Figure 4-4 Example of Flaring Occurring at Edges of a Cube Geometry

The 100% infill cube dataset included position data pertaining to the side walls of the cube is illustrated in figure 4-5. This may be since the nozzle has to spend more time on each layer due to needing to lay down more material and thus allowing for more time

to request coordinates. No data pertaining to the interior of the cube was collected and there was some observed flaring. If these datasets only represents the "trace" of the geometry and not the geometry itself, then the proposed model would be infeasible since no side channel data would correlate to the points seen in figures 4-3 and 4-5.

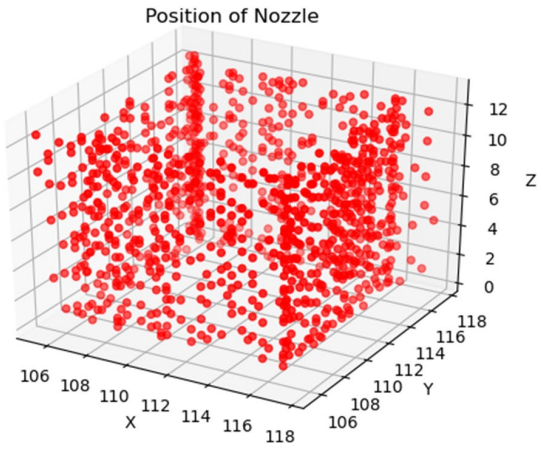

Figure 4-5 Coordinate History of the Nozzle During Printing of 100% Infill 1x1x1cm Cube

There were also some limitations to learn from. When requesting coordinates in the middle of a print, the coordinates would not be returned immediately. Rather there was an inconsistent lag time between requesting and receiving. The lag time lasted between 1-4 seconds after the command was given. Once again, this can be attributed to the fact that commands can only be processed once at a time. The printer needed to complete the command first before returning the coordinates. This dissonance in position data collection would make it almost impossible to identify which side channel data belongs to which coordinate.

CHAPTER 5. CURRENT AND VIBRATION STUDIES

With the evaluation of the temperature side channel showing little promise, especially with the Pronterface-python sampling methodology, there were thoughts of implementing a better sampling system. Therefore, the next sampling system would be a National Instruments PXIe chassis with higher sampling rate capabilities. Due to previous unpromising temperature results, it was decided that the NI system should be capable of collecting data from other side channels. The side channels the NI system could sample from were current and vibration. This section describes the feasibility of utilizing current and vibration side channels to predict geometric characteristics of printed geometries on the Ultimaker 2+.

5.1 Methodology

The methodology presented here will be constant throughout all the experiments mentioned in this chapter. Any exceptions to this methodology will be in the "methodology" section of the respective experiment.

5.1.1 Equipment

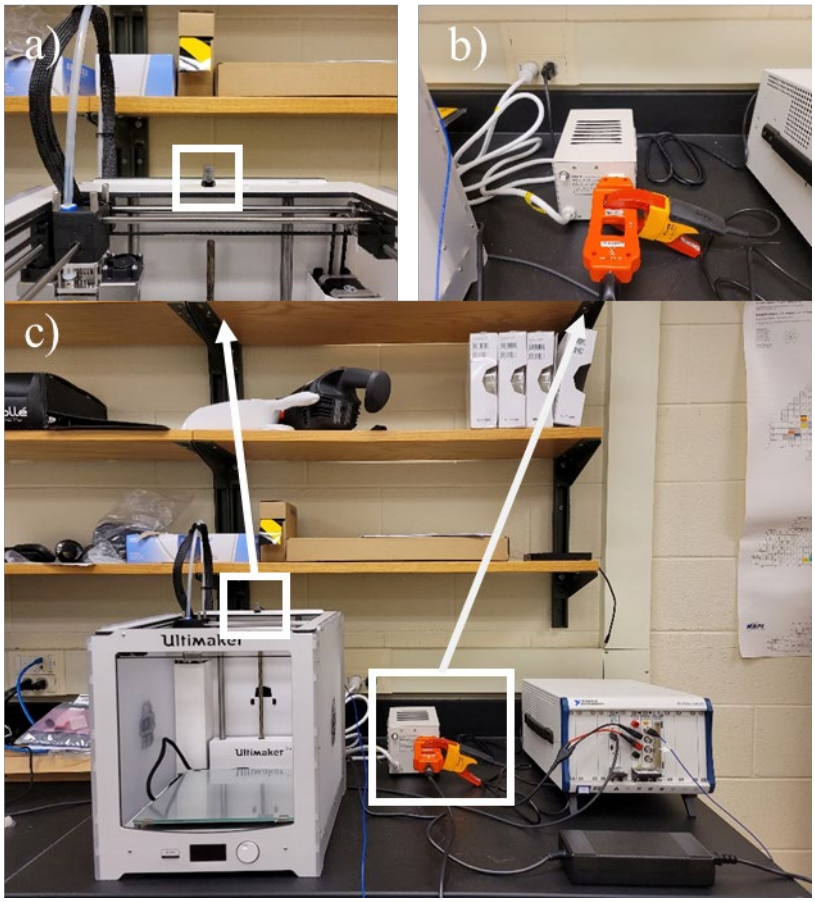

Figure 5-1 a) Piezoelectric Accelerometer b) Isolation Transformer, Line Splitter, Current Clamp c) Complete Experiment Setup

The AM machine of interest is the Ultimaker 2+ as shown in figure 5-1. The printer itself consists of a nozzle powered by an x motor and y motor, a glass substrate powered by a z-motor, and temperature controls for both the nozzle and substrate. The nozzle was fitted with a 4mm tip. On the back of the ultimaker, the filament roll is held in place, and was loaded with Ultimaker branded PLA.

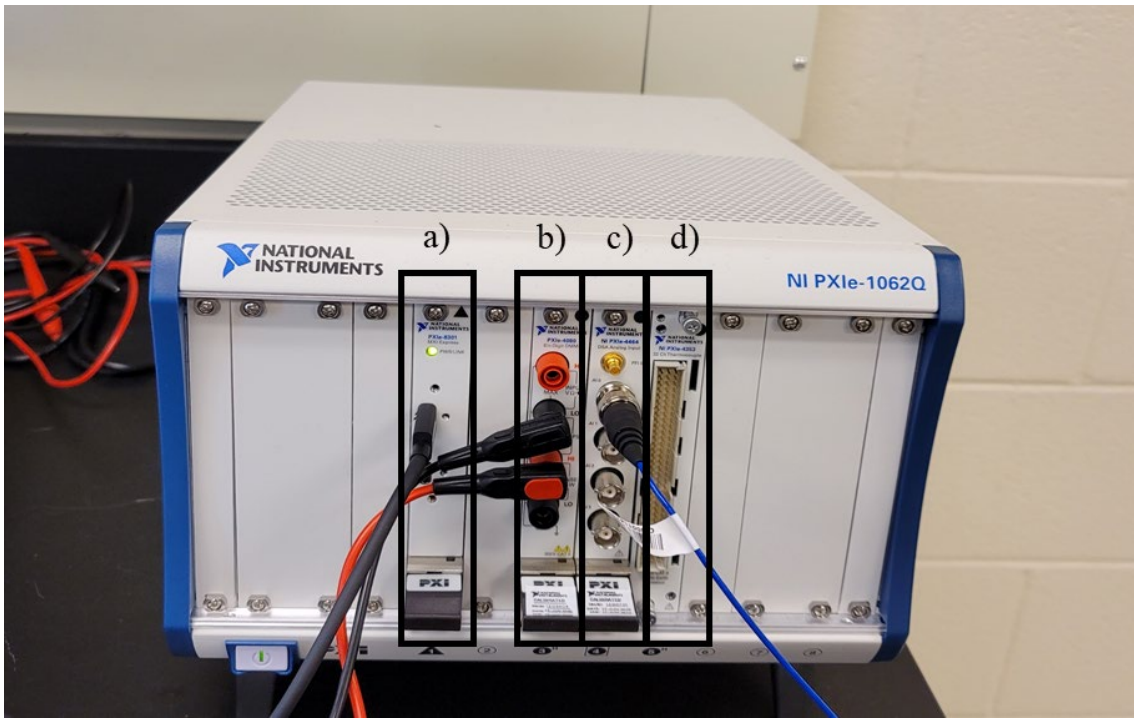

Figure 5-2 a) Thunderbolt 3 Module b) DMM c) Sound and Vibration Module d) Temperature Module

Different this time is the sampling method of which is a NI PXIe chassis and LabVIEW scripts. The chassis was comprised of several modules. In figure 5-2 from left to right: the first module is a thunderbolt 3 connectivity module. It allows for interfacing with any computer with thunderbolt 3 connectivity. The next is the digital multimeter. It functions like that of a handheld multimeter with the same connections. It can measure DC current, AC current, DC Voltage, AC Voltage, and resistance. It has a max precision of 6.5 digits and a max sampling rate of 1.8 MS/s. The next module is the sound and vibration module. It allows for connectivity to a piezoelectric accelerometer and offers a max sampling rate of 204.8 kS/s. The module outputted vibration in mV/g. The final module is a temperature in which allows for 32 channels of thermal couples to be connected, and was purchased in case of a revisit to the temperature side channel.

The piezoelectric accelerometer was purchased and used to capture vibrations emitted by the Ultimaker 2+ during the print process. It was connected via a low-noise banana plug cable to the NI chassis. It was mounted on top near the back middle of the Ultimaker frame via a command adhesive strip. Please refer to figure 5-1a for exact placement of the accelerometer.

A current clamp was used to measure current being drawn from the isolation transformer. The current clamp was connected via red and black cables to ports 2 and 3 on the NI chassis digital multimeter module. This enabled it to sample AC current and DC current.

Figure 5-3 Line Splitter

The current clamp was connected to a EXTECH 480172 AC line splitter. The line splitter allows for sampling current being drawn from the wall. The line splitter offers a means of sampling current without having to splice wires.

The line splitter was not connected directly to an outlet, rather it was connected to a Tripp Lite IS250HG isolation transformer. The isolation transformer allows the Ultimaker 2+ to draw upon a "clean" current signal as it can filter out noise generated by the wall. The isolation transformer was used to mitigate noise coming from the wall outlets.

The last essential piece of hardware that was used was a thunderbolt 3 cable that connected the thunderbolt 3 module to a computer. It allowed for connectivity between a computer and the NI chassis. LabVIEW was loaded onto the computer and used to interface with the NI chassis.

5.1.2 Data Collection

There are specific and consistent circumstances in which the data sampling was started. The most important circumstance was that the Ultimaker must have been in a state that allows for consistency during subsequent prints. The idle temperature of the Ultimaker upon startup is different than the idle state directly after a print has completed. Therefore a "dummy" print needed to be performed before real data could have been obtained. An example of differing idle conditions is the substrate temperature. The substrate temperature during the idle state when the printer has first turned on is approximately 20 degrees Celsius while substrate temperature during the idle state after a print has been completed is around 30 degrees Celsius.

The computer was preloaded with LabVIEW scripts. The LabVIEW user interface itself was used to initiate the sampling process. All samplings begin via human operator by pressing the "Run Continuously" button in the LabVIEW UI displayed in figure 5-4. Sampling started when the human operator observed that the nozzle reached 195 degrees Celsius.

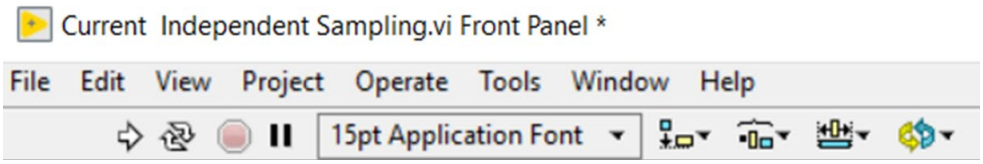

Figure 5-4 a) Run b) Run Continuously c) Abort Execution d) Pause

The end sampling point was designated as when the Ultimaker system has returned to its idle state. The idle state is defined as the nozzle being at x=0 and y=0, and the substrate being at z=0.

5.1.3 Data Processing

With the connections established, the computer connected would execute LabVIEW scripts based off which side channel was under evaluation. There were three variations: 1) concurrent sampling of current and vibration, 2) independent sampling of current, and 3) independent sampling of vibration. The raw side channel data would be dumped into in comma separated files (CSVs). The raw data needed to undergo post processing to ensure standardization of the datasets. Part of this post processing was alignment. There was no hard coded signal to start the collection process, rather a human needed to activate the sampling process. The sampling rate was on the order of milliseconds meaning that there

could have been large variances for t=0. To mitigate this variance, the datasets needed to be aligned. The alignment process began with identifying the startup and shutdown signals within the datasets. Both current and vibration side channels offered clear signatures that pertained to the beginning and the end of the process when plotted. Figure 5-5 distinguishes the start up and shut down signals for a vibration dataset.

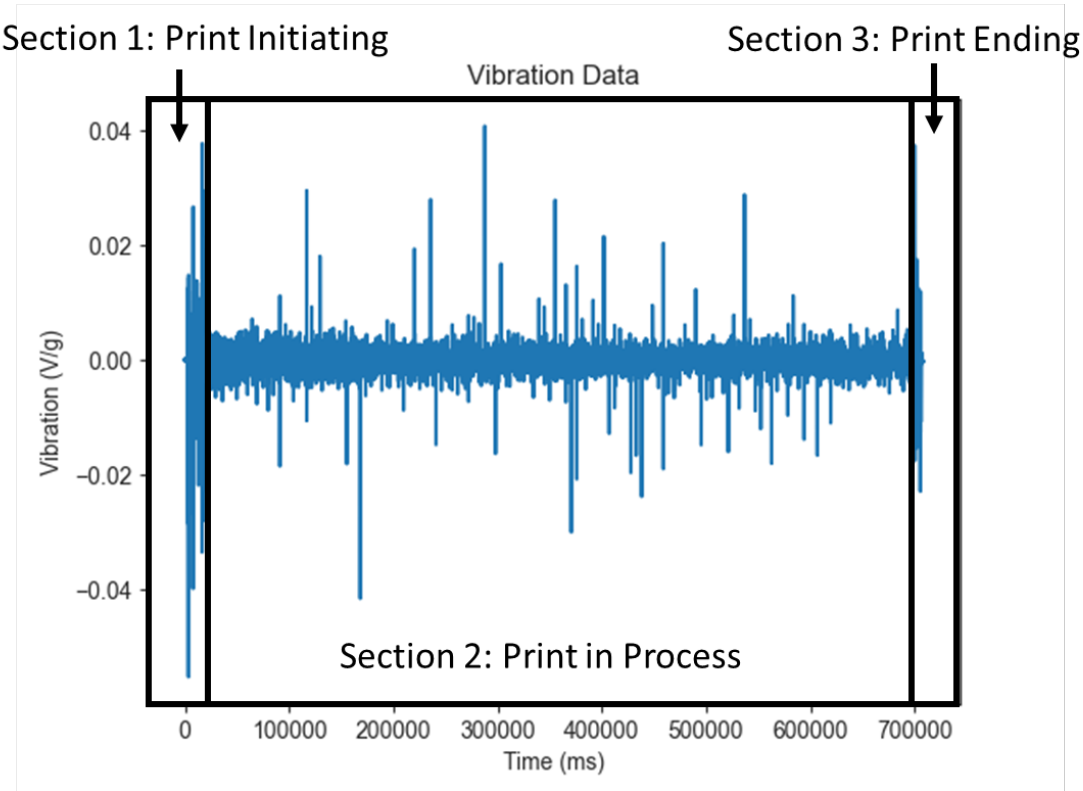

Figure 5-5 Start Up and Shut Down Signals for Vibration Data

The clear signals came in the form of "spikes" that represent the transition from an inactive state to an active or the transition from an active state to an inactive state. In figure 5-6 and figure 5-7 shows alignment by utilizing the shutdown process signal. To find these spikes, the python library matplotlib was to plot the entire time series dataset. Matplotlib allows for the user to specify a window to focus on, so the exact transition points can be

elucidated. Within these spikes, the transition point from an active state to an inactive state was used to manipulate datasets so that transitions would be in close in alignment as possible. This alignment process was done by hand and was determined by visual inspection.

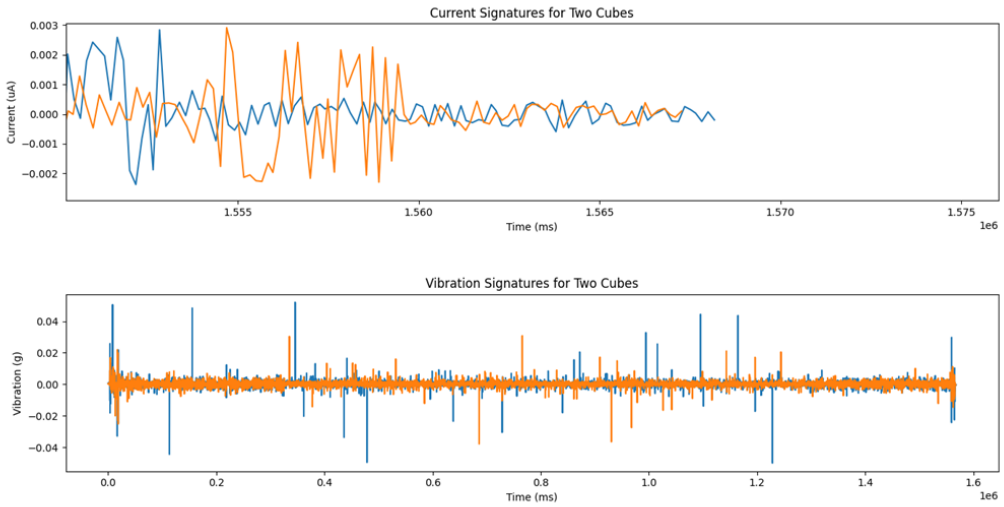

Figure 5-6 Current and Vibration Dataset Before Alignment

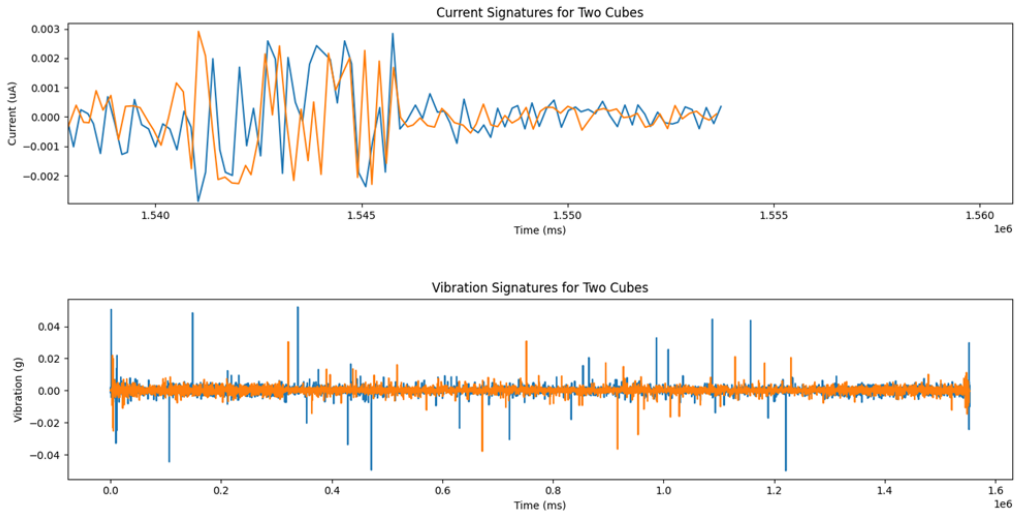

Figure 5-7 Current and Vibration Dataset After Alignment

5.2 Study 1: Time Dependent Current and Vibration

5.2.1 Motivations

In Chapter 3, the assumption presented was that for each timestep, there is a unique signature value at each timestep that only appears when a specific geometry is produced. this same assumption will be applied to current and vibration side channels. The goal is to show that current and vibration time series are unique to the geometries that produced them.

5.2.2 Methodology

5.2.2.1 Experimental Details

The geometries mentioned in figure 3-4 were reused for this experiment. The experiment span two days in which 9 total datasets were produced. Five cubes were produced on day one while two cubes and two cylinders were produced on day two. The purpose for day one was to test reproducibility while day two datasets were used to test for differences.

5.2.2.2 Data Collection

As this study samples both current and vibration concurrently, a custom LabVIEW script that can record data from both side channels was developed. Please refer to appendix section 2 for details. The sampling for vibration module was to 100,000 samples per second while the DMM module was set to 3.5 digits of precision. LabVIEW does not explicitly allow for the user to set the DMM sampling rate, rather the user needs to designate the

digits of precision. The lower of the digits of the precision, the higher the sampling rate. The script also ensured that current, vibration, and timestamp data were time-synced.

Please refer to section 5.1 for details about equipment and data collection procedures.

5.2.2.3 Data Processing

The dataset generated were subject to section 5.1.3 alignment and truncation procedures. The datasets were aligned using their shutdown transition points, and the datasets had their start up and shutdown signals omitted.

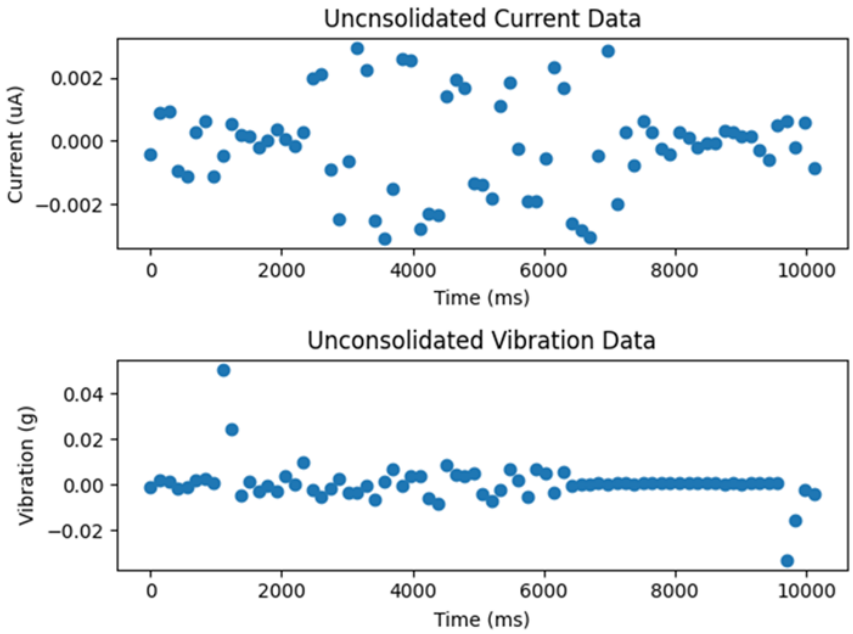

Figure 5-8 Unconsolidated Current and Vibration Dataset

After data processing operations discussed in section 5.1.3 occurred, the data was still subject to non-aligned intermittent data points. For instance, if point 200 in dataset one corresponded to t=10s, there was no guarantee that point 200 in dataset two would

correspond to t=10s. Essentially, this meant that some time steps would take longer or shorter than others. This phenomenon arose due to limitations of the NI system. To alleviate this, the datasets were consolidated into time-intervals. For example, a 10000-millisecond dataset with a designated 2000-millisecond time interval would be consolidated into a dataset of five points. All points within an interval would be averaged and the average of those points would serve as the representative point for that interval. The dataset presented in figure 5-8 was subject to this process. It was a 10000-millisecond dataset which was condensed into 2000 millisecond intervals. Figure 5-9 was the result of this consolidation. Each of the points in figure 5-9 has an associated standard deviation which will be used in this experiment as criteria for testing uniqueness. These standard deviations were used to evaluated how similar datasets were.

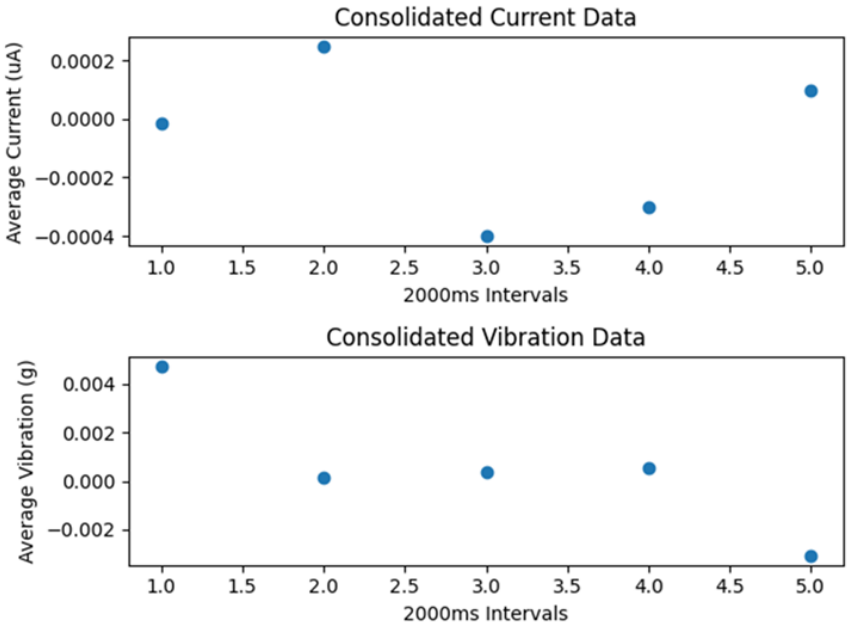

Figure 5-9 Consolidated Current and Vibration Dataset

5.2.2.4 Analysis

The standard deviations were essential to analysis of the results in this study. As mentioned earlier, the representative data points will be averages of their respective time intervals. Those averaged points will also have a standard deviation associated with the point. Point by point comparisons means there will be two averages and two standard deviations to compare for each interval. Using the smaller standard deviation between the two, a similarity criteria that was proposed was that if points were within one standard deviation of each other, they were consider similar.

5.2.3 Results

Table 5-1 Similarity Results Day 1

Similarity of Datasets (1σ)		
Comparison	**Similar Current Points (%)**	**Similar Vibration Points (%)**
Cube 1 vs. Cube 2	61.8	49.9
Cube 1 vs. Cube 3	57.1	51.5
Cube 1 vs. Cube 4	55.1	47.8
Cube 1 vs. Cube 5	60.1	50.2
Cube 2 vs. Cube 3	58.2	50.8
Cube 2 vs. Cube 4	55.6	49.8
Cube 2 vs. Cube 5	63.6	50.5
Cube 3 vs. Cube 4	56.1	49.8
Cube 3 vs. Cube 5	60.3	48.3
Cube 4 vs. Cube 5	58.9	50.0

Table 5-2 Similarity Results Day 2

Similarity of Datasets (1σ)		
Comparison	**Similar Current Points (%)**	**Similar Vibration Points (%)**
Cube 1 vs. Cube 2	59.45	38.96
Cyl. 1 vs. Cyl. 2	58.96	42.70
Cube 1 vs. Cyl. 1	59.64	47.87
Cube 1 vs. Cyl. 2	59.39	47.49
Cube 2 vs. Cyl. 1	58.75	45.83
Cube 2 vs. Cyl. 2	57.99	46.09

The results that table 5-1 presents initially seemed promising. It was expected that similar datasets should have similarities above 50%, and day one current similarities were approximately 60%. Vibration similarities were below 50%. When comparing the two side channels, the data seems to be suggesting that current may be more indicative of the geometry as a side channel as opposed to vibration. Even current had higher similarity values, the difference between the maximum value and the minimum was 8.5 which is higher compared to vibration similar difference of 3.7. This points to the fact that vibration may be a more consistent side channel and less subject to variation.

Table 5-2 elucidated the situation further by providing unexpected results. Expected was that the level of similarity should be lower than that of the cube versus cube comparisons but observed was that the current data similarity between the cube and cylinder were almost identical to the cube versus cube comparison. Day 2 results serve to invalidate the current time series data as a means of distinguishing geometries. Another

point of note is that day 2 vibrations for like geometry comparisons (i.e., cube vs cube and cyl vs cyl) were lower in similarity than dislike geometry comparisons. These values may have been outliers. The dislike comparisons are clumped closely together suggesting once again that it is more consistent than the current side channel.

There were also some complications to consider. The first was the use of standard deviations to test for similarity. It was an unstandardized metric to use since each interval would have their own definition of likeliness. Another complication was that the sampling rate was hindered by concurrent sampling. The vibration sampling rate was bottlenecked by the AC current sampling rate because AC current low sampling force the vibration module to slow down for the purpose of time-syncing. In addition, the generation of a timestamp slowed the sampling further because the script was responsible for time-syncing three pieces of data. The script needed to wait for data for the vibration data, the current, and the timestamp before it exports to the csv file.

5.3 Current Study 1

5.3.1 Motivation

Chapter 3 mentioned how the time series temperature distributions were used to test for uniqueness. The current side channel underwent the same comparison by having the current time-series collapsed into distributions. Relative frequency distributions were generated and tested to see if they are unique to the geometries that have generated those distributions.

5.3.2 Methods

5.3.2.1 Experimental Details

The geometries presented in figure 3-4 were used for this experiment. The cube geometry was used to produce two datasets, and the cylinder geometry was used to produce two datasets.

5.3.2.2 Data Collection

Please refer to section 5.1 for details on data collection. Please see appendix section 3 for details on the LabVIEW script used for this experiment.

5.3.2.3 Data processing

The current series data was collapsed in distributions via Python scripts and the Python pandas data processing library. The number of bins was arbitrarily picked to be 40. A relative distribution was used was to account for prints that do not have the same print times. Relative frequency offered a way to normalize all datasets for direct comparison.

5.3.2.4 Analysis

Once each dataset was in the form of a normalized distribution, they effectively served as vectors. Instead of analyzing those vectors by hand, a more hands off and rigorous analysis method will be employed here. An unsupervised machine learning was used to help derive conclusions from the datasets. K-means clustering was used because there was no need to generate a great number of datasets, and its ease of use. The algorithm groups samples together based on Euclidean distance.

$$d(A,B) = \sqrt{\sum_{i=1}^{n}(A_i - B_i)^2} \quad (1)$$

K-means clustering compares "centroids" to the samples that are past into the algorithm. It can utilize N centroids with N being defined with the user (section a in figure 5-10). These centroids are defined with random values at first. Once the sample is fed in, the sample will be compared to each N centroids until eventually it is grouped together with the centroid that it is closest to in terms of Euclidean distance (section b in figure 5-10). After grouping the sample, the centroid is then updated to represent the mean of the group they present (section c in figure 5-10). This process is completed until all samples have been classified and the centroids have reach convergence (section d in figure 5-10). Convergence in this case means that samples are no longer switching classifications. For this experiment, the algorithm was told to classify the data into two groups.

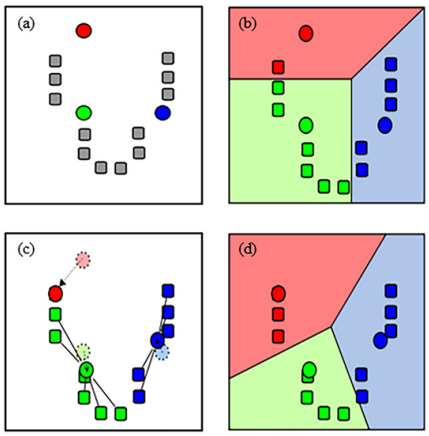

Figure 5-10 K-Means Clustering Process [16]

5.3.3 Results

Table 5-3 K-Means Clustering Labels for Current Datasets

K-means Classification				
Seed	**Cube 1**	**Cube 2**	**Cylinder 1**	**Cylinder 2**
1	0	0	1	1
2	1	1	0	0
3	1	1	0	0
4	0	0	1	1
5	0	0	1	1
6	0	0	1	1
7	1	1	0	0
8	1	1	0	0
9	0	0	1	1
10	0	0	1	1

What is expected is that algorithm will be able to place the cube geometries into one group and the cylinder geometries into another consistently regardless of seed. The labels are not necessarily important for this study. Rather, the labels for like geometries are always expected to be the same. This is what was observed for all 10 seeds in Table 5-3. It was able to classify cube and cylinder geometries into their respective groups with no overlap.

These results however should be taken with a grain of salt. This was a brief preliminary study with only about 4 samples, so more testing is needed for generalizations to be drawn; however, these results are promising for utilizing the current side channel for distinguishing what is being printed.

5.4 Current Study 2

5.4.1 Motivation

In all the previous experiments, there was an observation that there was a noticeable increase in current draw upon motor activation. That current draw could be measured and correlated to nozzle speeds. Knowing both the nozzle speed, the duration in which that speed lasted, and the motor that was activated can aid in developing a model that predicts the path filament was placed. For instance, the x-axis motor moving at 100 mm/s for second would deposit about 100mm worth of filament. This deduction can be repeated until the entire geometry is elucidated. The goal of this experiment is correlate AC current amplitudes to Ultimaker 2+ motor speeds.

5.4.2 Methods

5.4.2.1 Experimental Details

All motors on the Ultimaker 2+ all draw from the same current source. Because of this, it would be impossible to distinguish what motor was in use therefore this study will only be focused on sampling from the x-motor. The nozzle temperature will be kept at 20 degrees Celsius, and the substrate temperature will be set to 30 degrees Celsius.

The experiment included sampling from both single pass and multi-pass motions. This was done to test if there are any effects of switching directions during a print. For first part of the experiment, a single pass run was performed 5 times. The Ultimaker 2+ nozzle started at x=0 and be given commands to x=200. The nozzle was designated to move at 500 units/s while AC current amplitude values were collected. These single pass runs were

averaged and compared against 10 pass runs. The nozzle in 10 pass runs started at x=0 and were given commands to move to x=200. The nozzle would then move back and forth between these two coordinates 10 times. A pass was defined as a 200 unit traversal.

After ascertaining the effects of switching directions in the first experiment, the second part of the experiment continued to implement multiple passes. Multiple passes should have been more indicative of realistic behavior. The total amount of passes was set to 10. The speeds that were tested are 500 units per second, 2000 units per second, 5000 units per second, 7500 units per second, and 10000 units per second. For each speed, five 10 pass runs occurred.

5.4.2.2 Data Collection

Sampling of current side channel occurred the same as described in section 5.1. The independent current sampling script was set to 3.5 digits of precision for sampling. Please see appendix section 3 for details on LabVIEW script.

This experiment required a different method for activating the Ultimaker 2+. Instead of activating the Ultimaker 2+ with the UI, Pronterface was used again for its command line. The command line was used to give movement instructions to the nozzle. Please see figure 3-2 for Pronterface UI details. The specific instruction that was used was the “G1” command. For the “G1” command, the axis and coordinate, and the speed could be designated. An example of the command in use would be, “G1 X200 F500” which means move to x coordinate 200 with speed of 500 units/s.

It was highly impractical for a human operator to input movement commands in rapid succession therefore, a Python script utilized Pywinauto library to input g-code text strings and click buttons. This script let the user designate the number of passes, the coordinate, and the speed. Please refer to appendix 4 for details on the full script.

5.4.2.3 Data Processing

This experiment did not require dataset processing. The raw datasets were exported to csv files. Microsoft excel was used to view the datasets.

5.4.2.4 Analysis

The metric of interest was the amplitude of the AC current wave thus the maximum and the absolute value of the minimum of each dataset were ascertained. Thus, each dataset produced an AC current amplitude. The maximum current draw for each speed was plotted on a histogram to expose any potential patterns.

5.4.3 Results

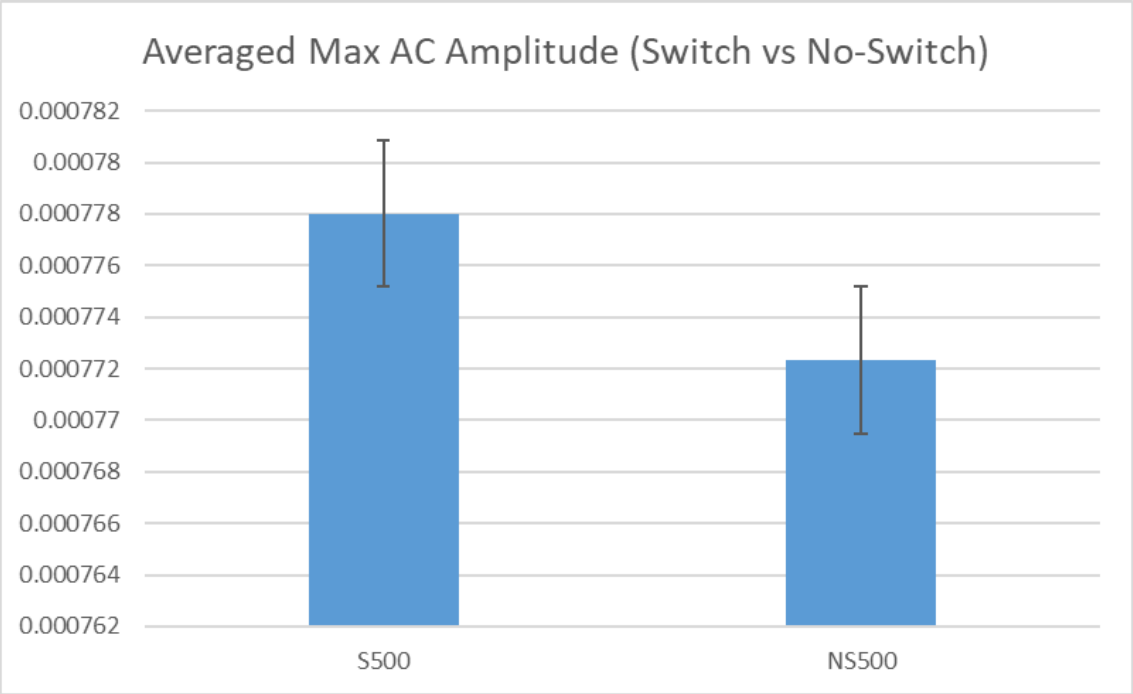

Figure 5-11 Average Max Current Draw (Switching vs No-Switching) With Speed Set to 500 Units/s

Figure 5-11 offers a comparison between the 500 unit per second one pass to the 500 unit 10 pass. Here, details concerning the nozzle switching directions were sought after. It was suspected that there would be a larger current draw when the nozzle had to switch directions. The one pass runs averaged a max current draw of 0.0007723 μA with a standard deviation of 1.88385E-05 while the 10 pass runs averaged a max current draw of 0.000778 with a standard deviation of 2.40555E-05. Based off the averages, multiple passes caused larger current spikes thus supporting the conclusion that having to switch directions causes larger current draws. However, considering the standard deviation, there was some overlap as the one pass mean plus its standard deviation (0.0007911) is within the same range as the 10 pass mean minus its standard deviation (0.0007539). There existed

the possibility that the trend observed in figure 5-11 may have been a coincidence. However, this trend will be assumed to be true for the part two for the experiment.

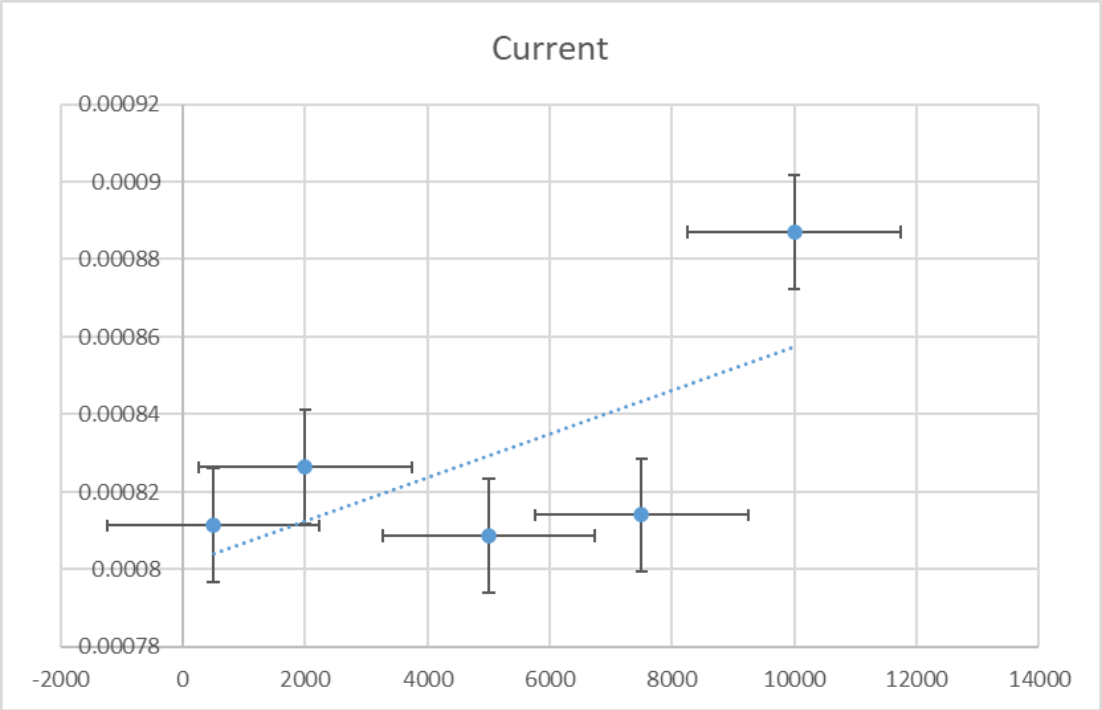

Figure 5-12 Maximum Current Draw Based on Motor Speed

Part two of the experiment started to look for correlations between AC current amplitude and the motor speed. It was expected that there would be a positive trend detailing that the larger to motor speed, a larger current draw signature would be sampled. Results revealed that there were extreme variations in the results. As figure 5-12 presents, it seems to suggest a linear trend subject to a lot of noise. Although all points may not be perfectly described by the dashed trend line, it is already promising that these averaged maximum results in the expected positive trend. Speeds 500 units/s, 2000 units/s, and 10000 units/s all seem to be in a very well-defined linear trend. Speeds 5000 units/s and 7500 units/s exhibited their own linear trend. This consistent positive linear trend suggests

that there is merit to the assumption that with greater nozzle speeds comes larger max current draws. The weak trend exhibited in this experiment may have to do with some of the limitations and complication that arose during this experiment.

The first observed major complication was that there was a varied sampling over time. This meant the for collection of data for longer period would miss more datapoints. It seemed that for high sampling rates, the system can endure short periods of sampling; however, during longer periods of time, higher sampling rates were difficult to maintain.

On the topic of missed datapoints, the slower sampling rates would have most likely missed critical points that would have exposed the actual amplitude of the AC wave. A higher sampling rate would have a better chance at capturing the true amplitude.

5.5 Vibration Study 1

5.5.1 Motivation

This study details how the vibration side channel can be used to predict the height of a component. Observation of the printing process revealed that large spikes seen in the vibration data could correspond to vibration spikes. By human observation, this seemed to be correlated to the printer transitioning from printing the infill to the printing the shell.

This transition happens once per layer meaning that it would be possible to estimate the number of layers in a print and multiply it by the layer height to get a prediction for the height of the object. This study will attempt to use the vibration side channel to predict the height of a printed geometry.

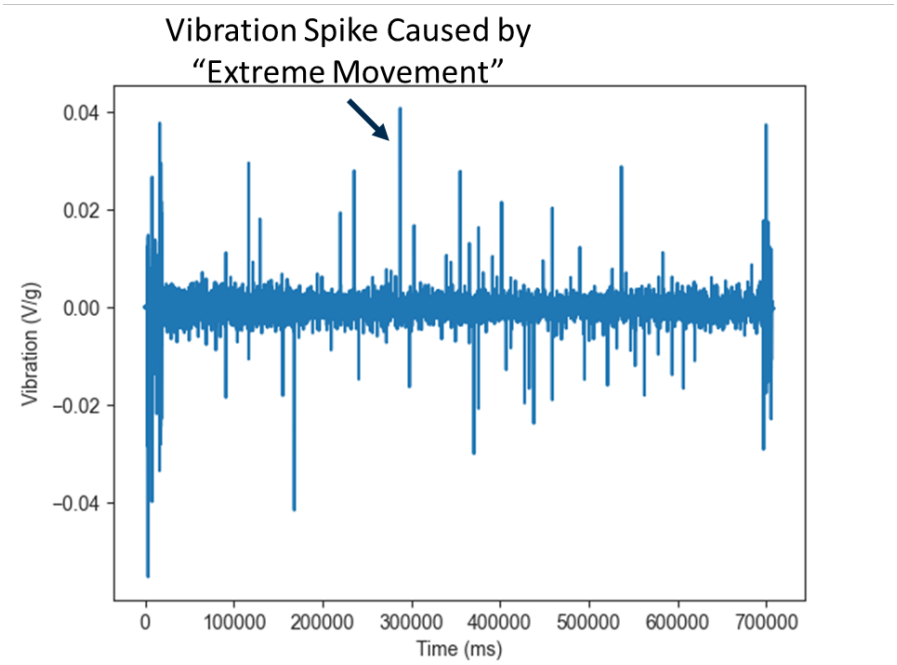

Figure 5-13 Vibration Dataset: "Spikes" Caused by Transition from Printing Infill to Printing Shell

Figure 5-13 points directly towards a vibration spike in a dataset. This spike was observed to be correlated with transitioning between printing the infill to printing the shell of the geometry. It can be noted that there are multiple vibration spikes, and all spikes were assumed to be a result of the transition. Also of note is the fact that spikes occur both in the positive direction and the negative direction.

5.5.2 Methodology

5.5.2.1 Experimental Details

The experiment utilized the cube geometry presented in figure 3-4. It will be scaled to make two additional geometries. The geometries used in this experiment are: 1) 1x1x1cm cube (medium), 2) 5x5x5mm cube (small), and 3) 2x2x2cm cube (large). The

1x1x1cm cube will be printed two times, the 5x5x5cm cube will be printed once, and the 2x2x2cm cube will be printed once.

5.5.2.2 Data Collection

A LabVIEW script that allowed for independent vibration sampling was implemented. The sampling rate was set to 100000 samples/s with 100 samples per channel. Please refer to appendix section 5 for the LabVIEW script. Please refer to section 5.1 for more details.

5.5.2.3 Data Processing

Alignment was not necessary in this study because datasets would not be superimposed. In addition, consolidation was also not needed since there was no comparison between time sensitive dataset. The dataset still needed to have the startup and shutdown signals omitted.

5.5.2.4 Analysis

To find the number of occurrences of spikes present within a dataset, thresholding was used. There would be a negative and a positive threshold would be applied, and any spikes that reach below or below the respective thresholds would be counted. The threshold tested are presented in table 5-4. All data analysis for this study was performed in excel, and the spike counting was performed by using the excel function “COUNTIF.”

5.5.3 Results

Table 5-4 Tested Thresholds and Number of Layers Detected

Thresholds	5x5x5mm Cube	1x1x1cm Cube 1	1x1x1cm Cube 2	2x2x2cm Cube
<-.002 or >.002	2354	3208	3258	5176
<-.004 or >.004	621	697	690	704
<-.006 or >.006	327	360	395	328
<-.008 or >.008	206	231	257	217
<-.010 or >.010	132	168	189	154
<-.012 or >.012	81	129	146	117
<-.014 or >.014	54	94	113	87

The geometries were set to a layer height of 0.1 mm. This means that 100 layers needed to be detected to compose a 1 cm tall object. The results revealed that there was a slight positive correlation when considering the .002 and .004 thresholds. All other thresholds detected less layers for the large cube contradicting the positive trend. The .012 and .014 threshold offered the most accurate results when detecting layers for the small and medium cubes. The .008 threshold gave the best results for the large cube. The best explanation for why the larger cube had less spike counted is because the large cube

allowed the nozzle to maneuver in a larger area. Therefore, it would not need to create such drastic movements when transition between the infill and the shell.

The data may suggest that there is different optimal threshold based on the size of the component; however, the most significant conclusion of this study may that for the .002 threshold, a clear positive linear trend occurs.

Some of the complication faced were that the higher speeds combined with the low sampling rate resulted in "missed" points. The low samplings speed failed to capture fully manifested spikes.

5.6 Vibration Study 2

5.6.1 Motivation

Much like current study 1, the vibration side channel was assessed to see if the generated distributions were unique to the geometries that produced them.

5.6.2 Methodology

5.6.2.1 Experimental Details

The geometries used are a r=.5cm z=1cm cylinder (cylinder), a 1x1x1cm cube (large cube), and a 5x5x5mm cube (small cube). Each geometry was printed five times resulting in a total of 15 datasets.

5.6.2.2 Data Collection

A LabVIEW script that sampled only vibration data was once again employed. The sampling rate was set to 100000 samples/s with 100 samples per channel. Please refer to appendix section 5 for the LabVIEW script. Please see section 5.1 for more details.

5.6.2.3 Data Processing

The data was exported to csv files and the points between the beginning and end of the process were identified and used to truncate the start up and shut down signals of each dataset leaving only data relevant to the print. The vibration datasets were then collapsed into relative frequency distributions using Python 3.7 and Python pandas data processing library. The number of bins was picked to be 50 arbitrarily. The designated range for the bins was -.0520 mV/g to .0520 mV/g.

5.6.2.4 Analysis

For analysis of the results, custom python scripts employing the sklearn library for machine learning results were used alongside Microsoft excel for distribution comparisons.

For this study, the results analysis was done using several methods. The first is using k-means clustering to group data points together. The clustering algorithm will display labels for each sample feed in. It was told to classify all samples into 3 groups. The k-means clustering algorithm depends upon seed, so multiple seeds were used to test for consistency in groupings. The k-means algorithm centroids were used to ascertain differences between the datasets.

5.6.3 Results

Table 5-5 K-means Clustering Labels for Vibration Distribution Datasets

Seed	A1	A2	A3	A4	A5	B1	B2	B3	B4	C1	C2	C3	C4	C5
1	1	1	1	1	1	2	2	0	2	0	0	2	0	0
2	0	0	0	0	0	2	2	1	2	1	1	2	1	1
3	1	1	1	1	1	2	2	0	2	0	0	2	0	0
4	1	1	1	1	1	2	2	0	2	0	0	2	0	0
5	1	1	1	1	1	2	2	0	2	0	0	2	0	0
6	1	1	1	1	1	2	2	0	2	0	0	2	0	0
7	0	0	0	0	0	2	2	1	2	1	1	2	1	1
8	1	1	1	1	1	2	2	0	2	0	0	2	0	0
9	1	1	1	1	1	0	0	2	0	2	2	0	2	2
10	0	0	0	0	0	2	2	1	2	1	1	2	1	1
11	1	1	1	1	1	0	0	2	0	2	2	0	2	2
12	1	1	1	1	1	2	2	0	2	0	0	2	0	0
13	1	1	1	1	1	2	2	0	2	0	0	2	0	0
14	1	1	1	1	1	0	0	2	0	2	2	0	2	2
15	0	0	0	0	0	2	2	1	2	1	1	2	1	1

One of the (1x1x1cm) cube datasets (B5) had to be omitted because of file corruption. It should also be noted that labels do not matter for this study instead what mattered was that the geometries all be classified into the same group. A confusion matrix for seed 1 is offered in table 5-6 to help with visualization of the results.

Table 5-6 Confusion Matrix for Seed 1 K-means Clustering Results

0	1	2	
4	0	1	Small Cube
1	0	3	Large Cube
0	5	0	Cylinder

Expected was that each geometry would be grouped together with like geometries. The most significant observation was that column A1-A5 were consistently group together which regardless of seed, and the cubes were never placed into the same group as the

cylinders. Figure 5-6 indicates that at least one sample from the large was placed into the small cube group while one small cube sample was placed into the large cube group. This phenomenon was observed across all seeds suggesting that 1x1x1cm cube distributions and 5x5x5mm cube distribution have an overlap. This was expected since the two cubes were generated based off the same base geometry, but only differed in scale. This suggest that there are parts of the vibration relative frequency distribution that can describe the geometry while other parts of the distribution can describe the scale.

To ascertain what details different parts of the distribution, describe, the centroids produced by the k-means clustering algorithm were used. The centroids serve as the mean representation of the group they are in. Seed 1 centroids distributions were used and subtracted for each other see where the differences lie. These absolute value of these differences were highlighted in figures 5-14 to 5-16.

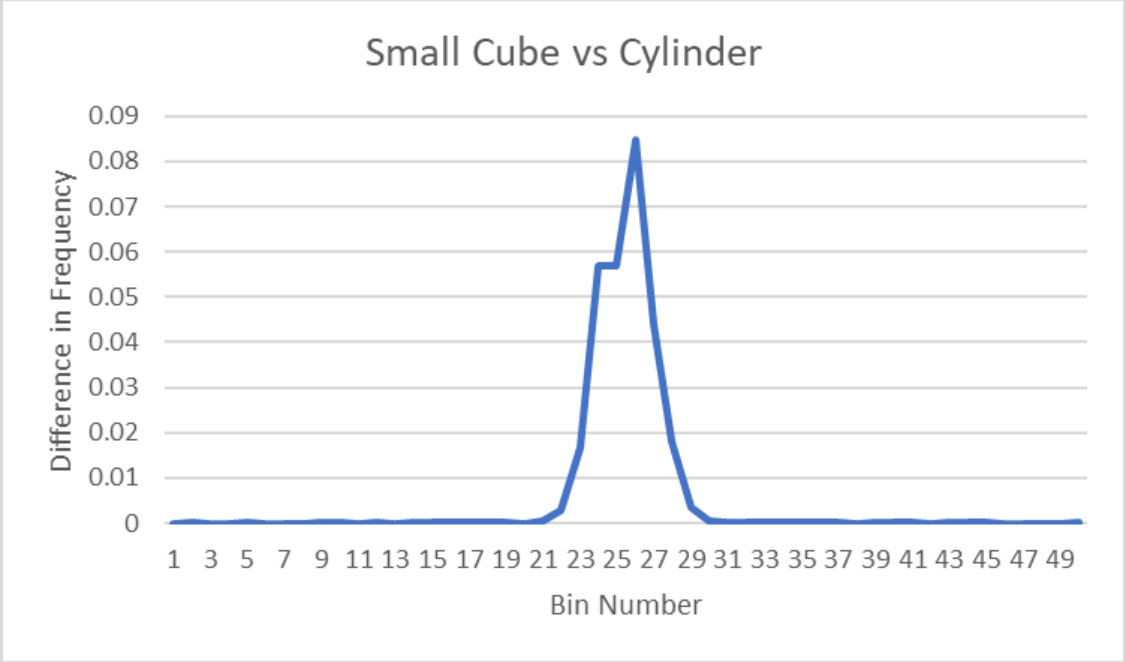

Figure 5-14 Small Cube Distribution Minus Cylinder Distribution

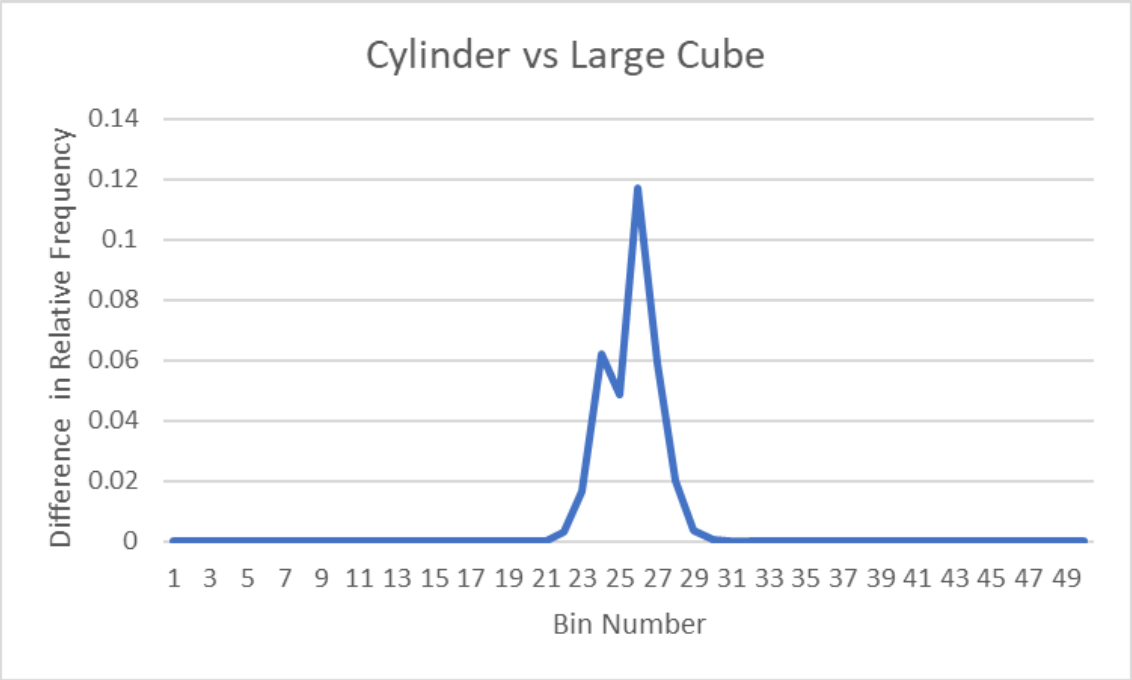

Figure 5-15 Average Cylinder Distribution Minus Large Cube Distribution

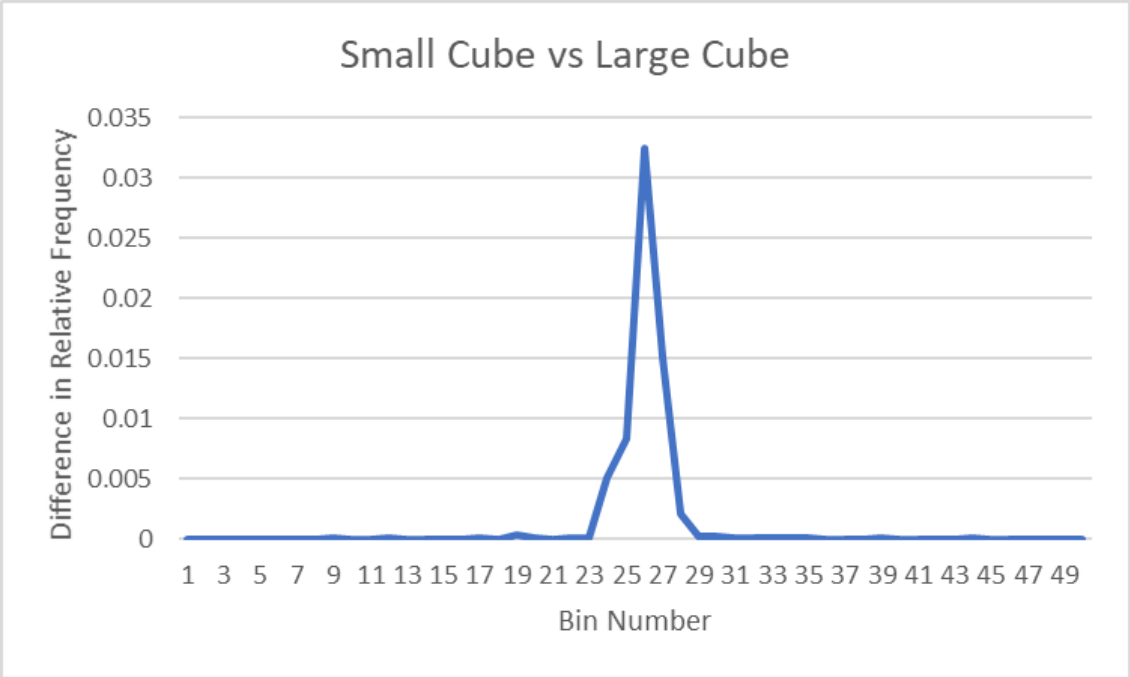

Figure 5-16 Small Cube Distribution Minus Large Cube Distribution

Figures 5-14 to 5-16 make it apparent that bins 24-26 were the most descriptive and indicative of the geometry being printed. Figure 5-14 and figure 5-15 should have the greatest highlighted differences as they represent cube versus cylinder distributions. It is of notice that the difference distribution in figure 5-14 is almost identical to 5-15. Of significance is that the differences between cubes and cylinders are consistent. Figure 5-16 represents the differences in a distribution when only size is varied. The distribution in this figure is unique and does not seem to have any overlap with figure 5-14 and 5-15

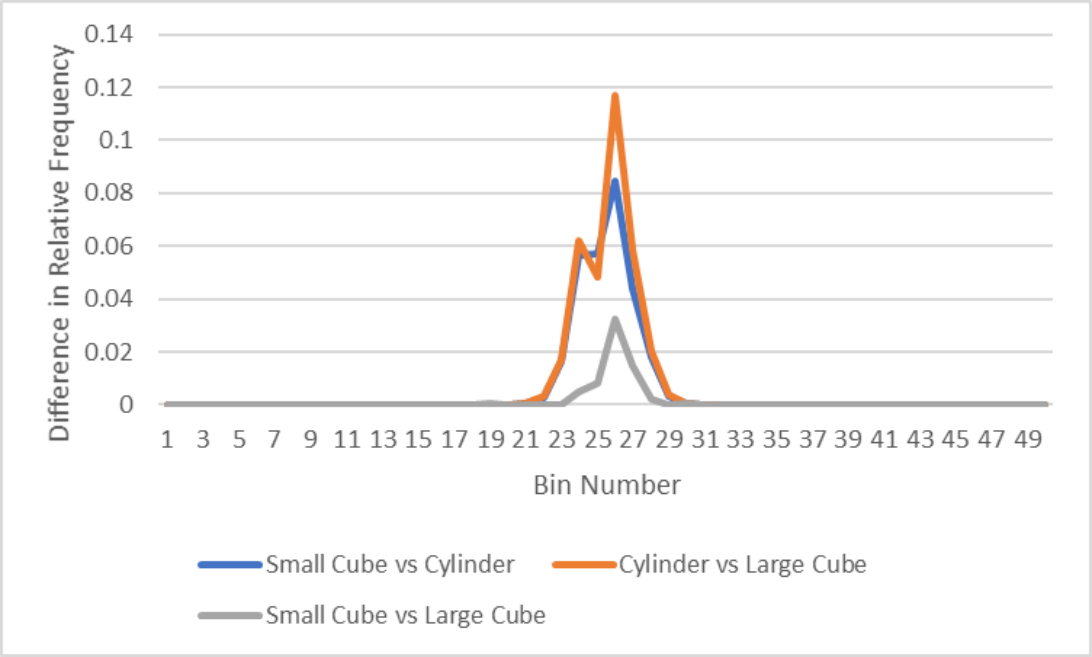

Figure 5-17 Differences in Relative Frequency: (Blue) 5x5x5mm Cube vs Cylinder (Orange) 1x1x1cm Cube vs Cylinder (Gray) 5x5x5mm Cube vs 1x1x1cm Cube

Figure 5-17 was generated to show that the differences between the cubes are less than that of the cylinder geometry. These differences might confirm that vibration distributions are capable of both distinguishing between geometry and distinguishing between scale.

However, this study had some limitations and complications to consider. This study only had 14 samples making it difficult to extrapolate results and to conclusively say that vibration distributions can describe geometries. As mentioned in other studies, the sampling rate may have been too low resulting in “missed” datapoints. Overall, these results should be used as a motivator to further experiment and to find definite patterns.

CHAPTER 6. CONCLUSION

6.1 Summary

This work attempts to utilize temperature, current, and vibration side channels to derive geometric characteristics about additively manufactured components for a thermoplastic system. It was concluded that both the current side channel and temperature side channel, at least for the Ultimaker 2+ system and this sampling method, is not capable of predicting geometric characteristics.

The current side channel showed promise when considering distributions. Although a small study, k-means clustering was able to distinguish between geometries consistently into their groups indicating that there might be unique current distributions for each geometry. The second study attempted to correlate current to AC waves resulted in an exhibited a weak trend; however, all data points seem to be positively correlated.

Utilizing vibrations to predict layer heights offers two main conclusions: 1) there was a positive trend exhibit when implement the .002mV/g and the .004mV/g thresholds, indicating that there is some correlation between layer height and the number of counted spikes, and 2) there seems to be an optimal threshold based off the size of an object. Vibration distributions offered some promising results. K-means clustering was able to use vibration distributions to distinguish between samples that varied geometry and scale. The sample size for this study was 15, so generalizations cannot be made.

In all, this work has demonstrated that it is feasible to use current and vibration side channels to predict geometric characteristics about an object manufactured on a FDM

machine. This demonstration can be deemed as a harmful and good. Harmful because it validates the threat that proliferators can potentially steal nuclear critical geometries by tapping side channel, and good because this work serves as the first steps toward developing monitoring tools to examine what proliferators are making enabling overseers to intervene before proliferators can manufacture something harmful.

6.2 Future Work

Below details some of the possible next steps for this research and some hindsight evaluations of the experiments performed.

6.2.1 Temperature

Temperature experiments presented may benefit from a higher sampling rate system since the Pronterface-python sampling methodology only offered 1 sampler per second at most. A higher sampling rate exposes intermittent points and may expose more patterns in the dataset. Therefore, the next progression would be to perform an experiment with the higher sampling rate NI temperature module to affirm or deny the results presented in chapter 3.

Even though the temperature side channel did not produce great results, that may be a result of the platform itself. As the literature alludes, temperature plays a much more important role in metal AM than it does in thermoplastics. Future work could transition away from thermoplastic materials.

In addition, those studies collect temperature information of AM systems through a different means. Instead of collecting raw temperature information, they collect

temperature information utilizing cameras whether that be optical cameras or thermal cameras. A possible next step may be to install a thermal camera above the Ultimaker 2+.

When considering current and vibration side channels, their time series data was condensed into distributions and then feed into the k-means algorithm. It may be worth to implement the same analysis with temperature distributions to test if the temperature side channel is truly non-usable.

6.2.2 Current

Current studies could have been improved if a constant analysis scheme was kept through the entire work. For instance, in chapter 3 an absolute differencing analysis was used to test for likeliness while in chapter 5 a standard deviation-based analysis was used to test for likeliness. It would be worthwhile implementing the absolute differencing analysis instead because standard deviations are subject to change. This would be applied to time-series data.

For distribution analysis studies, the sampling rate could be improved by getting rid the LabVIEW code used to generate a timestamp. The data is already time-insensitive, so omission would make the process more streamlined.

Current study 1 could be improved by scaling up to see if can properly group multiple geometries, that vary in shape, scale, and material. The Ultimaker 2+ is capable of handling multiple materials aside from PLA. In addition, many more samples should be manufactured for experiments so that generalization can be made.

Current study 2 results produced a linear trend that could be used for predicting the nozzle speed. For further validation, experiments could be performed in which max current draw is once again measured and then used in tandem with the linear trend to predict nozzle speed. Utilizing the predicted nozzle speed multiplied by the duration the movement lasted for, a prediction for how far the nozzle travelled can be produced. This prediction can be compared against

Furthermore, current study 2 could have produced more tangible results if the user were able to sample from three different channels. This next progression would then be to splice into specific wires that pertain to each individual motor. It would offer three channels and would eliminate the "overlap" phenomenon where signals would be superimposed if multiple motors were in use.

6.2.3 Vibration

The initial vibration study (current and vibration study) used a standard deviation-based scheme to evaluate similarity. In hindsight, an absolute difference analysis should have been applied as standard deviations are subject to change and can't be used as a means of comparison.

For both vibration experiments, getting rid of timestamps could have increased sampling rate as both analyses performed does not depend upon time sensitive data. An increase in higher sampling rate may have exposed more spikes and offered more definitive results in vibration study 1. For vibration study 2, it may be worthwhile to test the effects of different sampling rates to see how low the sampling rate can go to still have "distinguishable geometries.

APPENDIX A. PYTHON SCRIPTS AND LABVIEW SCRIPTS USED FOR EXPERIMENTS

A.1 Pronterface-Python Sampling

```
import time
import win32gui
from pywinauto.application import Application

app = Application().connect(title='Pronterface')
p= open("position_data_set1_cube.txt","w+")
t= open("temp_data_set1_cube.txt","w+")
ti= open("time_data_set1_cube.txt","w+")
app.Pronterface.menu_select("File ->Clear")
starttime=time.time()
timeout = time.time() + 60*30*1  # 60 seconds times 60 meaning the script will run for 1
hr
while time.time() <= timeout:
    textbox = app.Pronterface.window(title_re="Here").set_text('M114')
    app.Pronterface.send.click_input()
    cursor_position = win32gui.GetCursorPos()
    time.sleep(2.5)
    time_data = time.time() - starttime
    position = app.Pronterface.window(title_re=">>> M114").texts()
    temp = app.Pronterface.window(title_re="T:").texts()
    textbox.set_text("Here")
    p.write(str(position) + "\n")
    t.write(str(temp) + "\n")
    ti.write(str(time_data) + "\n")
    app.Pronterface.menu_select("File ->Clear")
    if cursor_position != win32gui.GetCursorPos():
        break
    time.sleep(4 - ((time.time() - starttime) % 4))
p.close()
t.close()
ti.close()
app.Pronterface.menu_select("File ->Clear")
```

A.2 Current and Vibration Sampling LabVIEW Script

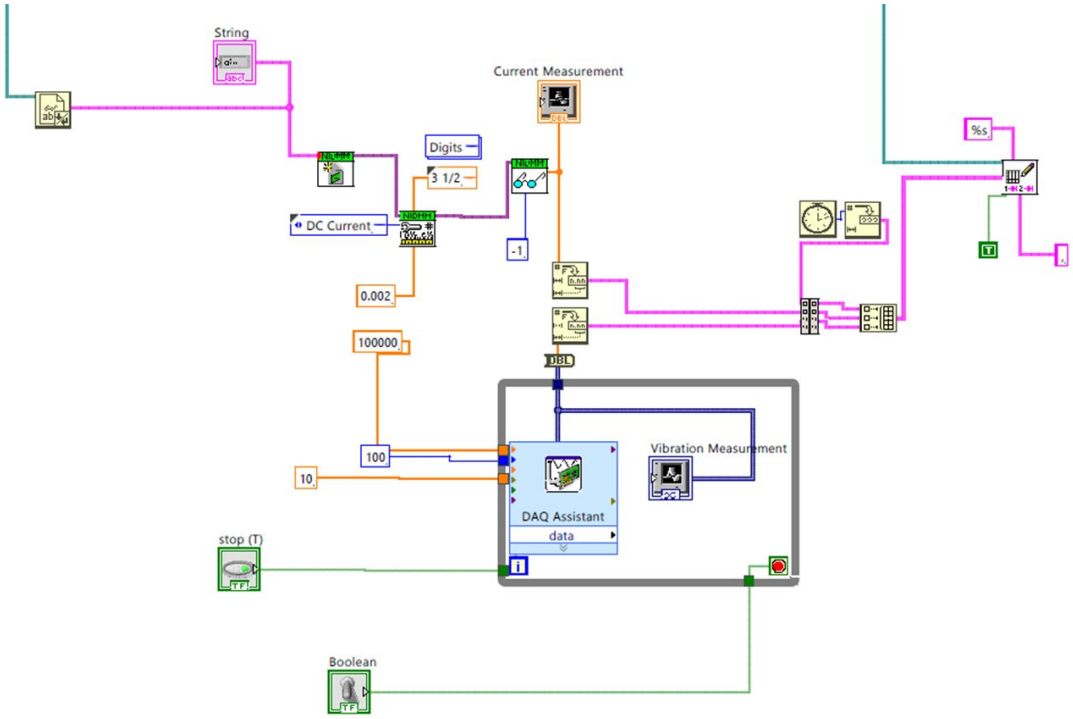

A.3 Current Sampling LabVIEW Script

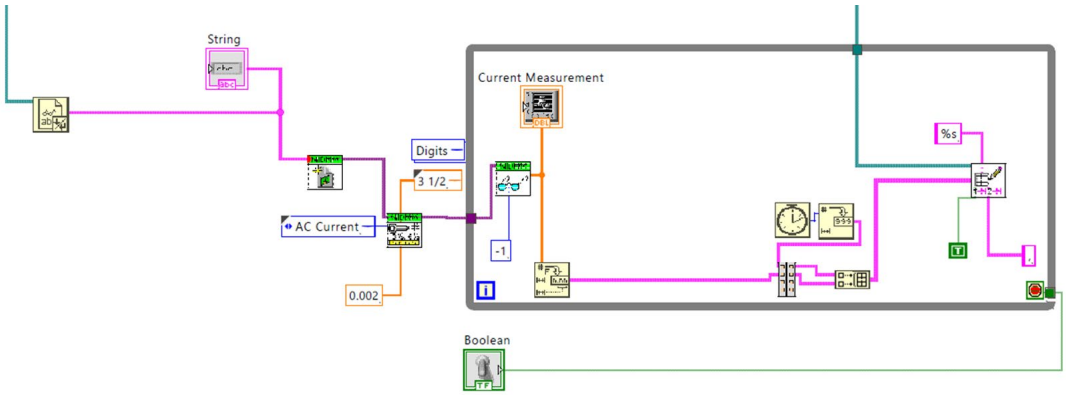

A.4 Pronterface-Python Ultimaker 2+ Nozzle Command Script

```
import time
import win32gui
from pywinauto.application import Application

app = Application().connect(title='Pronterface')

app.Pronterface.menu_select("File ->Clear")


passes = 10


cmd1 = 'G1 X200 F30000'
cmd2 = 'G1 X0 F30000'

for i in range(0,passes):
    if (i+1) % 2 != 0:
        textbox = app.Pronterface.window(title_re="Here").set_text(cmd1)
    else:
        textbox = app.Pronterface.window(title_re="Here").set_text(cmd2)
    app.Pronterface.send.click_input()
    cursor_position = win32gui.GetCursorPos()
    textbox.set_text("Here")
```

A.5 Vibration Sampling LabVIEW Script

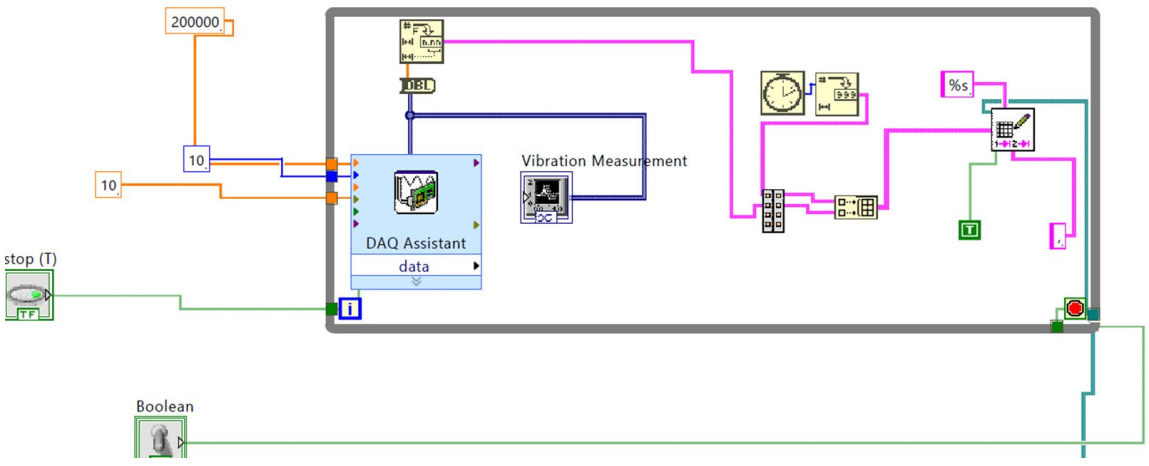

REFERENCES

[1] Vaezi, Mohammad & Seitz, Hermann & Yang, Shoufeng. (2012). A review on 3D micro-additive manufacturing technologies. The International Journal of Advanced Manufacturing Technology. 67. 10.1007/s00170-012-4605-2.

[2] Kruth, J-P., et al. "Binding mechanisms in selective laser sintering and selective laser melting." Rapid prototyping journal (2005).

[3] Singh, M., Haverinen, H.M., Dhagat, P. and Jabbour, G.E. (2010), Inkjet Printing—Process and Its Applications. Adv. Mater., 22: 673-685. https://doi.org/10.1002/adma.200901141

[4] Zhang, Y., He, X., Du, S. et al. Al2O3 Ceramics Preparation by LOM (Laminated Object Manufacturing). Int J Adv Manuf Technol 17, 531–534 (2001). https://doi.org/10.1007/s001700170154

[5] Kroenig, Matthew & Volpe, Tristan. (2015). 3-D Printing the Bomb? The Nuclear Nonproliferation Challenge. The Washington Quarterly. 38. 7-19. 10.1080/0163660X.2015.1099022.

[6] Bergeron, Andrew & Crigger, James. (2018). Early progress on additive manufacturing of nuclear fuel materials. Journal of Nuclear Materials. 508. 10.1016/j.jnucmat.2018.05.058.

[7] Arnaud Bertsch et al 2003 J. Micromech. Microeng. 14 197

[8] Gonzalez, J.A. & Mireles, Jorge & Lin, Y. & Wicker, R.B.. (2016). Characterization of ceramic components fabricated using binder jetting additive Manufacturing technology. Ceramics International. 42. 10.1016/j.ceramint.2016.03.079.

[9] Bandyopadhyay, A., Panda, R.K., Janas, V.F., Agarwala, M.K., Danforth, S.C. and Safari, A. (1997), Processing of Piezocomposites by Fused Deposition Technique. Journal of the American Ceramic Society, 80: 1366-1372. https://doi.org/10.1111/j.1151-2916.1997.tb02993.x

[10] Jialin, Yang. (2017). Selective Laser Melting Additive Manufacturing of Advanced Nuclear Materials V-6Cr-6Ti. Materials Letters. 209. 10.1016/j.matlet.2017.08.014.

[11] Al Faruque, Mohammad Abdullah, et al. "Forensics of thermal side-channel in additive manufacturing systems." University of California, Irvine (2016).

[12] M. A. Al Faruque, S. R. Chhetri, A. Canedo and J. Wan, "Acoustic Side-Channel Attacks on Additive Manufacturing Systems," 2016 ACM/IEEE 7th International Conference on Cyber-Physical Systems (ICCPS), 2016, pp. 1-10, doi: 10.1109/ICCPS.2016.7479068.

[13] Wu, Mingtao & Song, Zhengyi & Moon, Young. (2019). Detecting cyber-physical attacks in CyberManufacturing systems with machine learning methods. Journal of Intelligent Manufacturing. 30. 10.1007/s10845-017-1315-5.

[14] Sturm, Logan & Williams, Christopher & Camelio, Jamie & White, Jules & Parker, Robert. (2017). Cyber-physical vulnerabilities in additive manufacturing systems: A case study attack on the .STL file with human subjects. Journal of Manufacturing Systems. 44. 154-164. 10.1016/j.jmsy.2017.05.007.

[15] Li, Zhixiong & Zhang, Ziyang & Shi, Junchuan & Wu, Dazhong. (2019). Prediction of Surface Roughness in Extrusion-based Additive Manufacturing with Machine Learning. Robotics and Computer-Integrated Manufacturing. 57. 10.1016/j.rcim.2019.01.004.

[16] Multi-attribute k-means clustering for salt-boundary delineation from three-dimensional seismic data - Scientific Figure on ResearchGate. Available from: https://www.researchgate.net/figure/The-schematic-illustration-of-the-k-means-clustering-of-12-observations-into-three_fig1_328859982 [accessed 15 Apr, 2021]